

Changes in Area of Stubai Glaciers  
analysed by means of Satellite Data  
for the GLIMS Project

DIPLOMARBEIT

ZUR ERLANGUNG DES AKADEMISCHEN GRADES

MAGISTRA DER NATURWISSENSCHAFTEN

AN DER

LEOPOLD-FRANZENS-UNIVERSITÄT

INNSBRUCK

eingereicht von

IRENE SCHICKER

INNSBRUCK, MÄRZ 2006



# Abstract

The extent of glaciers in the Stubai Alps, Tyrol, Austria, was mapped using satellite data for the Global Land Ice Measurements from Space (GLIMS) Project. Data of two satellite systems were applied, namely two ASTER images of 23 August 2003 covering the southern and northern part of the study region and a Landsat 5 Thematic Mapper (TM) image of 30 September 1985. Algorithms recommended by the GLIMS group were used for analysing glaciers and their extent. For analysing debris covered glacier areas two different approaches were applied, based on a ratio of image channels in the near and mid - infrared. In the ASTER images the ratio of band 3 to band 4 was used, in the Landsat image the ratio of band 4 to band 5. The next step optionally one of the two possible algorithms was applied. One algorithm used a combination of spectral bands, the other algorithm used the hue component of the IHS transformation.

The derived glacier areas of 1985 and 2003 were compared to the areas from the Austrian Glacier Inventories of 1969 and 1997, based on aerial photogrammetry. In the Landsat image all glaciers except one, OE 16 NN, could be mapped. In the ASTER image 29 of the 117 Stubai glaciers could not be mapped due to clouds and cast shadow. Between 1969 and 2003 14 glaciers had disappeared. These 14 glaciers were taken into account for calculation of area changes. The total glacier area of the Stubai Alps in the Landsat TM image of 1985 amounted to 62.2 km<sup>2</sup>, the corresponding area in the Austrian Glacier Inventory of 1969 was 63.05 km<sup>2</sup>. Between 1969 and 1985 the total change in area for the Stubai glaciers was minus 1.35% in respect to 1969. The decrease in area between 1985 and 1997 of 13.2% is in agreement with the general glacier retreat in the Alps at the end of the 1980's and during the 1990's. For quantifying the glacier retreat up to 2003, the areas of the 88 glaciers were considered that were not obscured by clouds in the ASTER images. This includes also the 14 small glaciers that had disappeared between 1997 and 2003. The area of these 88 glaciers amounted to 54.1 km<sup>2</sup> in 1969, 54.4 km<sup>2</sup> in 1985, 47.2 km<sup>2</sup> in 1997 and 36.9 km<sup>2</sup> in 2003. The retreat between 1969 and 2003 was 32% of the 1969 area, with significant retreat starting after 1985 and accelerating between 1997 and 2003, in accordance with increasing summer temperatures towards the end of the period. Between 1997 and 2003 the area decreased by 22% relating to 1997. Large glaciers showed less relative change than small glaciers. Thus the area of Sulzthal Ferner, one of the largest glaciers in the region, decreased from 4.16 km<sup>2</sup> in 1969 to 3.51 km<sup>2</sup> in 2003 (minus 15.6%), whereas the small glaciers (< 0.1 km<sup>2</sup>) lost 89% in area.



# Contents

<b>Abstract</b>	<b>i</b>
<b>Contents</b>	<b>ii</b>
<b>1 Introduction</b>	<b>1</b>
1.1 Study region . . . . .	1
1.2 Outline . . . . .	3
<b>2 The GLIMS - Project and Relevant Glacier Characteristics</b>	<b>5</b>
2.1 GLIMS - Global Land Ice Measurements from Space . . . . .	5
2.1.1 What GLIMS is About . . . . .	5
2.1.2 The Structure of GLIMS . . . . .	6
2.1.3 Data and Algorithms . . . . .	7
2.1.4 Transfer Specifications . . . . .	10
2.2 Glacier Characteristics . . . . .	12
2.2.1 Glacier Types and Morphological Zones . . . . .	12
2.2.2 Mass Balance . . . . .	15
2.3 The Use of Remote Sensing in Glacier Mapping . . . . .	18
2.3.1 Optical Properties of Ice and Snow . . . . .	18
<b>3 Database</b>	<b>21</b>
3.1 Satellite Data . . . . .	21
3.2 Digital Elevation Model - DEM . . . . .	26
3.3 The Austrian Glacier Inventory . . . . .	27
<b>4 Methods and Algorithms</b>	<b>29</b>
4.1 Algorithms of the GLIMS - Project . . . . .	29
4.1.1 Geolocation and Orthorectification . . . . .	30
4.1.2 Manual Mapping of Glacier Boundaries . . . . .	31
4.1.3 Spectral Ratio . . . . .	33

4.1.4	Snow classification by the NDSI -Normalised Difference Snow Index . . . . .	34
4.1.5	Unsupervised Classification . . . . .	36
4.1.6	Supervised Classification . . . . .	37
4.1.7	Debris . . . . .	38
4.1.8	Identification of Glacier Basins . . . . .	40
4.1.9	Glacier ID - Points . . . . .	40
4.2	Other Algorithms used . . . . .	41
4.2.1	IHS-colour-space Transformation . . . . .	41
4.2.2	PCA-Principal Component Analysis . . . . .	43
4.2.3	Central Flowlines . . . . .	43
4.3	Summary on Methods used . . . . .	44
<b>5</b>	<b>Results</b>	<b>47</b>
5.1	Comments on Glacier Identification . . . . .	47
5.2	Analysis of Results . . . . .	48
5.2.1	Statistics of Glacier Size and Area at Given Dates . . . . .	48
5.2.2	Area Changes 1985 - 2003 . . . . .	50
5.3	Comparison with the Austrian Glacier Inventories . . . . .	54
5.3.1	Comparison of the Landsat Data with the Austrian Glacier Inventories . . . . .	54
5.3.2	Comparison of the ASTER Data with the Austrian Glacier Inventories . . . . .	56
5.4	Snow Coverage on Glaciers in 1985 . . . . .	60
<b>6</b>	<b>Summary and Conclusion</b>	<b>61</b>
	<b>Bibliography</b>	<b>64</b>
	<b>A Software</b>	<b>69</b>
	<b>B Tables</b>	<b>71</b>
	<b>C EASI scripts</b>	<b>83</b>
	<b>D Example of Transfer Files</b>	<b>87</b>

# Chapter 1

## Introduction

Measurements of changes in glacier area in Austria have been carried out since the beginning of the 19<sup>th</sup> century. Methods in glacier mapping changed since that time. The USGS-led project GLIMS, Global Land Ice Measurements from Space, has the objective to monitor glaciers in many regions of the world with the same method based on satellite images (see <http://www.glims.org>). An advantage of satellite based glacier mapping is less expenditure of human labour in obtaining data and large area coverage compared to the other methods. Data for analysing glacier areas are taken from various satellites. The preferred sensor is the Advanced Spaceborne Thermal Emission and reflection Radiometer (ASTER) sensor onboard the TERRA satellite, one of NASA's Earth Observing System (EOS) family. In this thesis data of the Landsat 5 Thematic Mapper (TM) satellite are also used.

The methods applied in this thesis are based on the GLIMS Algorithm Working Group (Kääb, 2004) algorithms and some additional algorithms, e.g. IHS transformation. Glacier areas of 1985 and 2003, mapped in satellite images for all the Stubai mountain range, are compared.

The second objective of this thesis was the comparison of the satellite derived glacier outlines of 1985 and 2003 with glacier data of the Austrian Glacier Inventories of 1969 and 1997.

### 1.1 Study region

The Stubai Alpen mountain range is located in the western part of Austria, in the federal state of Tyrol. It is part of the central eastern alps, south west of Innsbruck between Wipptal and Ötztal. A part of the southern Stubaital belongs to South Tyrol, Italy.

Stubaital ranges from 1300 m to 3507 m in height. 117 glaciers in total are located in

Stubai mountain range, the largest of which are concentrated in the southern part. The northern part of Stubaital is nowadays only sparsely glaciated. The largest glacier in this area, Übeltalgletscher, is located in South Tyrol and not considered in this thesis. 110 peaks in Stubaital are higher than 3000 m. A glacier ski resort, which has slopes on five glaciers, is located in Stubaital. 88 of the 117 glaciers located on the Austrian part of the Stubai mountain range are exposed in northern direction. The directions of the other 29 glaciers range from east to west. Figure 1.1 shows the western part of Austria with glaciers in black. Temperature data of Obergurgl, located in Ötztal, are shown in figure 5.2.

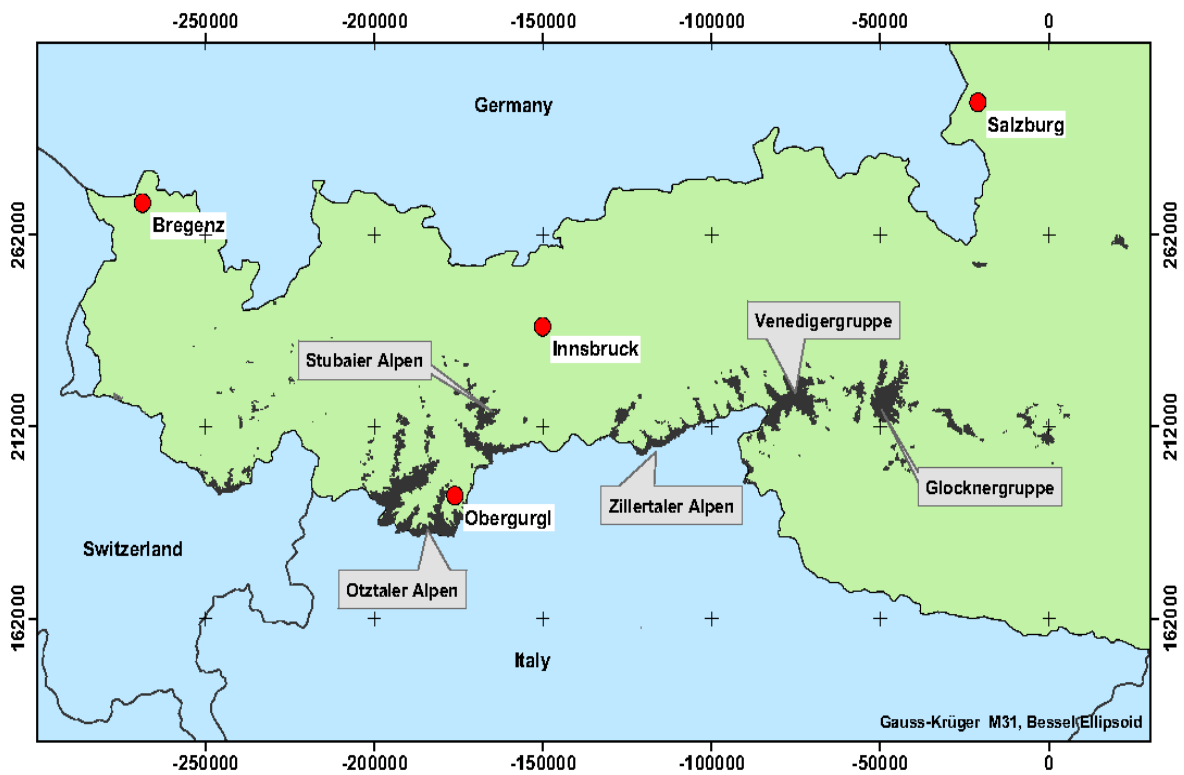


Figure 1.1: Western Austria with glacier areas.

Figure 1.2 shows a closer look of the Stubaital mountain range. The Austrian part of the Stubai Alps extends from the Austrian/Italian border in the south to the Innvalley in the north. In the west the boundary is the Ötztal and in the east it's the Wipptal.

The main drainage basins in Stubaital area are the Ötztaler Ache in west, the Mellach in the north and the Simmingbach and the Ruetzbach, which flow into the Sill.





Figure 1.2: Stubaital area in a closer look with the main drainage basins of the Stubai glaciers (<http://www.berge-tirol.at>). Stubaial area is inside the line in magenta, glaciated areas are marked with the turquoise lines.

## 1.2 Outline

Chapter 2 gives an overview of GLIMS and its guidelines. Described are, amongst others, algorithms and data transfer specifications. Chapter 2 describes also briefly relevant glacier characteristics and the use of remote sensing in glacier mapping. The satellite sensors Landsat 5 TM and ASTER are described in Chapter 3. The used Digital Elevation Model (DEM) and the Earth model, BMN M28, are described in part 2 of Chapter 3. A short introduction to glacier mapping history and basic information on the Austrian Glacier Inventories of 1969 and 1997 are given in part 3 of Chapter 3. In Chapter 4 methods for analysis of glaciers in satellite images and for deriving glacier boundaries are described. In addition to glacier areas, maps of debris covered ice and firn/snow areas were produced. The results of the work

and comparison of changes between 1985 and 2003 are summarised in Chapter 5. Changes between satellite derived glacier areas and glaciers areas of the Austrian Glacier Inventories of 1969 and 1997 are discussed in part 2 of Chapter 5. In Chapter 6 the methods used and the results are summarised.

## Chapter 2

# The GLIMS - Project and Relevant Glacier Characteristics

In the first part of this chapter the project GLIMS and its principles (structure, algorithm, transfer specification) are described. The second part gives a brief introduction on glacier characteristics that are of relevance for this work.

### 2.1 GLIMS - Global Land Ice Measurements from Space

#### 2.1.1 What GLIMS is About

GLIMS is a worldwide project to monitor and measure changes in the global land ice using remote sensing methods. The project started in 1995.

Primary data base for GLIMS are images of the ASTER (Advanced Spaceborne Thermal Emission and reflection Radiometer) instrument onboard the EOS Terra satellite. Additional satellite data used in this project are from the Landsat - satellites and the Radarsat system.

The goal of GLIMS is to compile an up to date inventory of glaciers with standardised parameters ( e.g. area changes, transient snow lines, flow velocity) covering as many glacier areas of the world as possible. The inventory is stored in a GIS database located at the NSIDC (National Snow and Ice Data Centre). The data of the inventory are freely accessible via the internet (<http://www.glims.org>).

## 2.1.2 The Structure of GLIMS

The data centre of GLIMS is located at the USGS (United States Geological Survey), it coordinates 23 regional centers. These regional centers are responsible for a database of the glaciers in their region which should be as complete and up to date as possible. They are also expected to provide information about the climate and physiographic data of the region (e.g. topography).

The stewards of a regional center coordinate the processing of glaciers for the given region. Figure 2.1 shows the organisation structure of GLIMS.

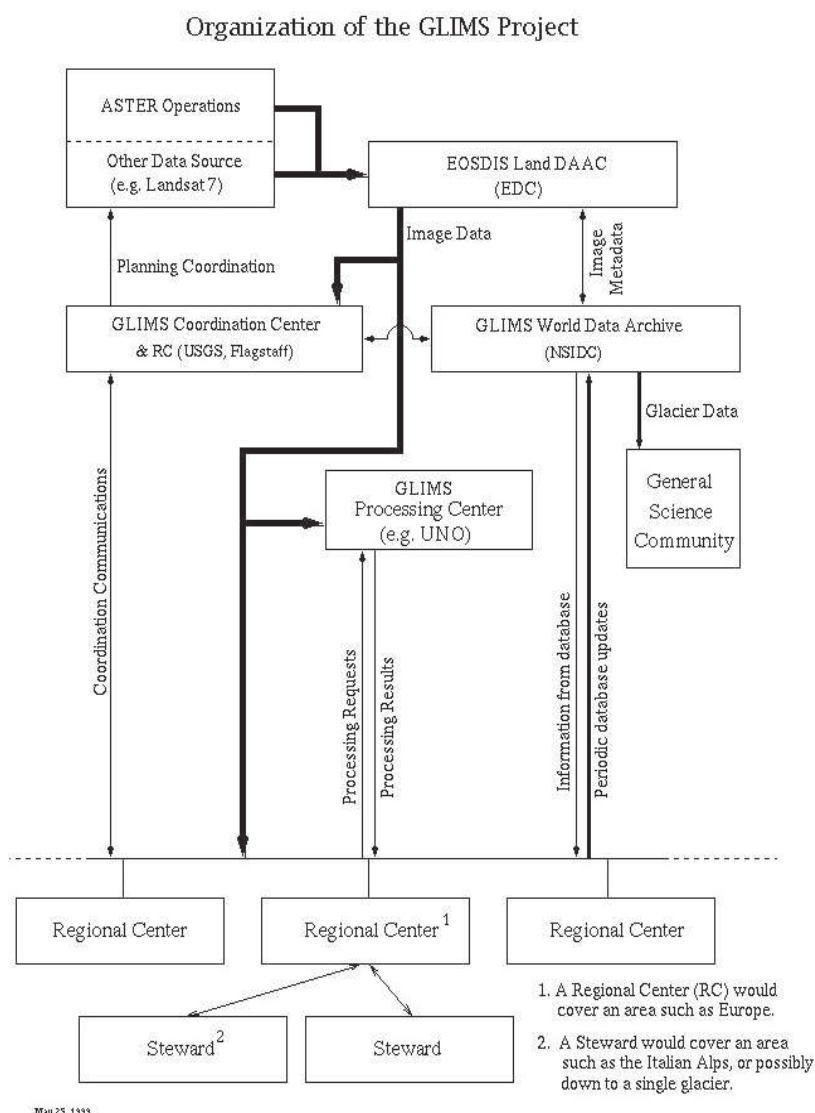


Figure 2.1: Organisation structure of the GLIMS - project. RC = regional center, EOS = EROS Data Centre, NSIDC = National Snow and Ice Data Centre, UNO = University of Nebraska at Omaha (from <http://www.glims.org/>)

### 2.1.3 Data and Algorithms

#### Data

Originally, it was planned to use for GLIMS almost exclusively data from the ASTER (Advanced Spaceborne Thermal Emission and reflection Radiometer) instrument. For the period before the launch of the EOS Terra satellite in 1999 data of the Landsat - satellites and Radarsat - satellite or also other satellite images are used. Because of inadequate coverage of some glacier regions by ASTER, images from other satellites are also used after the EOS Terra was launched. The preferred data products of the ASTER instrument are level 1A and level 1B data.

The processing software can be chosen individually by the regional center, but the processed glacier data have to be sent in standardised format to USGS.

#### Algorithms

The GLIMS group has provided tutorials and how-to-do guides on the retrieval of glacier areas and other characteristics on their web page. 4 tutorials are discussed in this subsection.

The **GLIMS Algorithm Working Group** (Kääb, 2004) lists various options:

1. Multispectral classification for mapping glacier areas
  - Manual glacier boundaries: on contrast enhanced FCC (False Colour Composit) image either pixel by pixel (raster based) or vector based cursor tracking of glacier boundaries.
  - Ratio: ratio of two image channels to obtain a glacier mask
  - NDSI (Normalised Difference Snow Index): based on differences in spectral properties of snow in VIS and MIR
  - Unsupervised classification: ISODATA clustering with various input bands
  - Supervised classification: requires training areas according to specified object classes (e.g. forest, town, shadow, ice) and final classification with available classifier (e.g. Maximum-Likelihood)
2. Multidimensional classification
  - Debris: classification of debris covered glacier ice using a combined approach of the ratio glacier map, a vegetation map from hue component of the Landsat TM channels 3, 4 and 5 and a slope map from a DEM

- glacier boundaries delineation from a DEM: creating a centreline of the glacier and using an algorithm that searches out from the centreline for V-shaped grooves
- Glacier basins: separating large ice masses into individual glaciers using their watersheds (produced with the DEM for the area)

### 3. Ice velocity measurements

- IMCORR: uses two coregistered images and a series of input parameters; this program is used to measure the glacier velocities. It is an open source software and can be downloaded from the NSIDC homepage (<http://www.nsidc.org>).
- CIAS (Correlation Image Analyser): image pyramid matching using double cross-correlation in feature space; also for measuring ice velocity

### 4. DEM (Digital elevation model) creation

- DEMs obtained from ASTER stereo bands using PCI Orthoengine
- ASTER DEMs by McKinnon/Kääb
- ASTER DEMs using LH Systems SOCET SET

The **University of Alberta** (Copeland, 1995) is the regional center of the high arctic regions of Canada. They recommend in their guide to use the GIS software ArcView but also apply for classification the same algorithm as the GLIMS Algorithm Group.

**Morphological Description of Glaciers** The **GLIMS Regional Centre 'Antarctic Peninsula'** (Rau et al., 2005) at the University of Freiburg uses the following morphological classification steps:

- Primary classification: classify the glaciers into morphological types by distinct units (e.g. continental ice sheet, ice-field, valley glacier, mountain glacier)
- Form: describes the outline of a glacier (e.g. compound basin, simple basin, niche, ice apron)
- frontal characteristic: describes the frontal characteristic of the glaciers (e.g. piedmont, lobed, calving)

- Longitudinal characteristics: encodes the description of the glacier surface profile (e.g. regular, cascading, ice fall)
- Major source of nourishment (e.g. avalanches, super-imposed ice, snow drift)
- Tongue activity (e.g. marked retreat, stationary, known surge)
- Moraine code 1 (in contact with present day glacier) e.g. no moraines, terminal moraines.
- Moraine code 2 (moraines farther downstream) e.g. terminal moraines, lateral and/or medial moraine, push moraine.
- Debris coverage of tongue (debris free, partly debris covered, mostly debris covered, completely debris covered)

The **GLIMS Analysis Tutorial** of Raup and Khalsa (Raup and Khalsa, 2005) is also a good guideline for glacier classification and satellite data processing.

Another guideline for processing is the **Processing plan for GLIMS** of Bruce Raup (Raup, 1996). He advises in this early document (some parts may have been changed meanwhile) to determine for each glacier:

- Glacier ID
- glacier area
- area of accumulation zone
- glacier length (along centreline arc)
- glacier width as function of position along centreline
- Orientation of glacier
- multipoint arc describing the position of the glacier terminus
- multipoint arc describing the position of the snow line

### 2.1.4 Transfer Specifications

To guarantee platform independence, the information from the regional centers and their glaciers have to be in ESRI shapefile format. The ESRI shapefile format is used by multiple softwares (e.g. Open Source) in the GIS (Geographic Information System) based world. These glacier shapefiles will then be sent to the NSIDC.

Another advantage of the ESRI shapefiles besides the platform independence is the minimisation of programming work and that later changes in the database can be made easier.

The transfer specifications used in the GLIMS project are described in table 2.1.

Shapefile name	Mandatory	Type*	Geometry
session.shp	y	1,5,11,or 15	outline of region, or point in middle of region, or point where regional center is located
glaciers.shp	y	1 or 11	point location of glacier
segments.shp	y	3,5,13 or 15	line segments
vec_sets.shp	n	1,5,11 or 15	centre of mass (point)of vector set, or convex hull around vectors
vec_points	n	3 or 13	two - point vector arcs
histograms.shp	n	1 or 11	point at centre of glacier
ancillary.shp	n	1 or 5	
images.shp	y	5	polygon made of footprint, or part of mosaic made up from this image
point_meas.shp	n	1 or 11	point measurements

Table 2.1: List of shapefiles for GLIMS Data transfer. \* shapefile types. (after <http://www.glims.org>)

The session shapefile contains information about the entire analysis session such as the regional center ID, time of analysis completion, analyst's name, data source and description of processing.

The glacier shapefile holds the information of the individual glacier.

In the segment shapefile are the debris outlines, glacier outlines, rock outlines, centerlines and also the position uncertainties.

The image shapefile contains information of the image used in the analysis.



These 4 shapefile types are mandatory. The `vec_sets`, `vec_points`, histograms, ancillary and `point_meas` shapefiles are not mandatory. The `vec_sets` and `vec_points` shapefiles hold information of the displacement of the vectors, the histograms shapefile contains area-elevation histograms, the ancillary shapefile contains basic metadata about additional datasets and the `point_meas` shapefile holds information about point measurements done on the individual glacier.

As an example a submission for Alpeiner Ferner in the Stubai Alps is used in this thesis; the suffix `.shp` stands for the geographic points, the suffix `.dbf` contains the attributes, `.shx` is an index file and the bibliographic files have the suffix `.en` (see Appendix D):

- `alpeinerferner_session.shp` (plus `.dbf`, `.shx`)
- `alpeinerferner_glacier.shp` (plus `.dbf`, `.shx`)
- `alpeinerferner_outlines.shp` (plus `.dbf`, `.shx`)
- `alpeinerferner_centrelines.shp` (plus `.dbf`, `.shx`)
- `alpeinerferner_snowlines.shp` (plus `.dbf`, `.shx`)
- `alpeinerferner_debrislines.shp` (plus `.dbf`, `.shx`)
- `alpeinerferner.en`

Also included in the submission are the image files if possible in geoTIFF format.

## 2.2 Glacier Characteristics

### 2.2.1 Glacier Types and Morphological Zones

#### Types of Glaciers

The shape, form, size and the interaction with the local topography defines the type of a certain glacier. Since the World Glacier Inventory (WGI) exists and contains glacier data in many regions, but still is incomplete, an exchange and share of the data with the GLIMS archive is of interest. For this reason the morphological glacier parameters in the World Glacier Monitoring Service (WGMS) database were adopted for the GLIMS database. The following categories in glacier classification, according to the WGMS glacier classification system (after Rau et al., 2005) , are used for the GLIMS - Project:

- continental ice sheet
- ice field
- ice cap
- outlet glacier
- valley glacier
- mountain glacier
- glacierete and snowfield
- ice shelf
- rock glacier

In the Alps the dominant glacier types are the valley and mountain glaciers. Ice fields can be found in many region of the world e.g. in Patagonia and Norway. Ice caps are compact ice masses, which often have outlet glaciers (e.g. Barnes Icecap). The following figures show examples of some glacier types. The glaciers are located in Stubaital, in Switzerland, Ötztal and Norway. Figure 2.2a shows the Daunkopf Ferner, a glacierete, located in the southern Stubaier Alps. The Daunkopf Ferner is one of those glaciers which split into several parts. 2.2b shows the Habicht Ferner, a cirque glacier, which was split in 2003 into 2 parts but has recovered. In summer, 2005, the 2 parts are connected again. 2.2c shows the Daunkogel Ferner on the right side and the Schaufel Ferner on the left side of the picture. Both are mountain

glaciers. These 2 glaciers are part of the Stubaier Glacier Ski Area. Figure 2.2d shows the Sulzenau Ferner on the right side and the Grünau Ferner, also mountain glaciers.

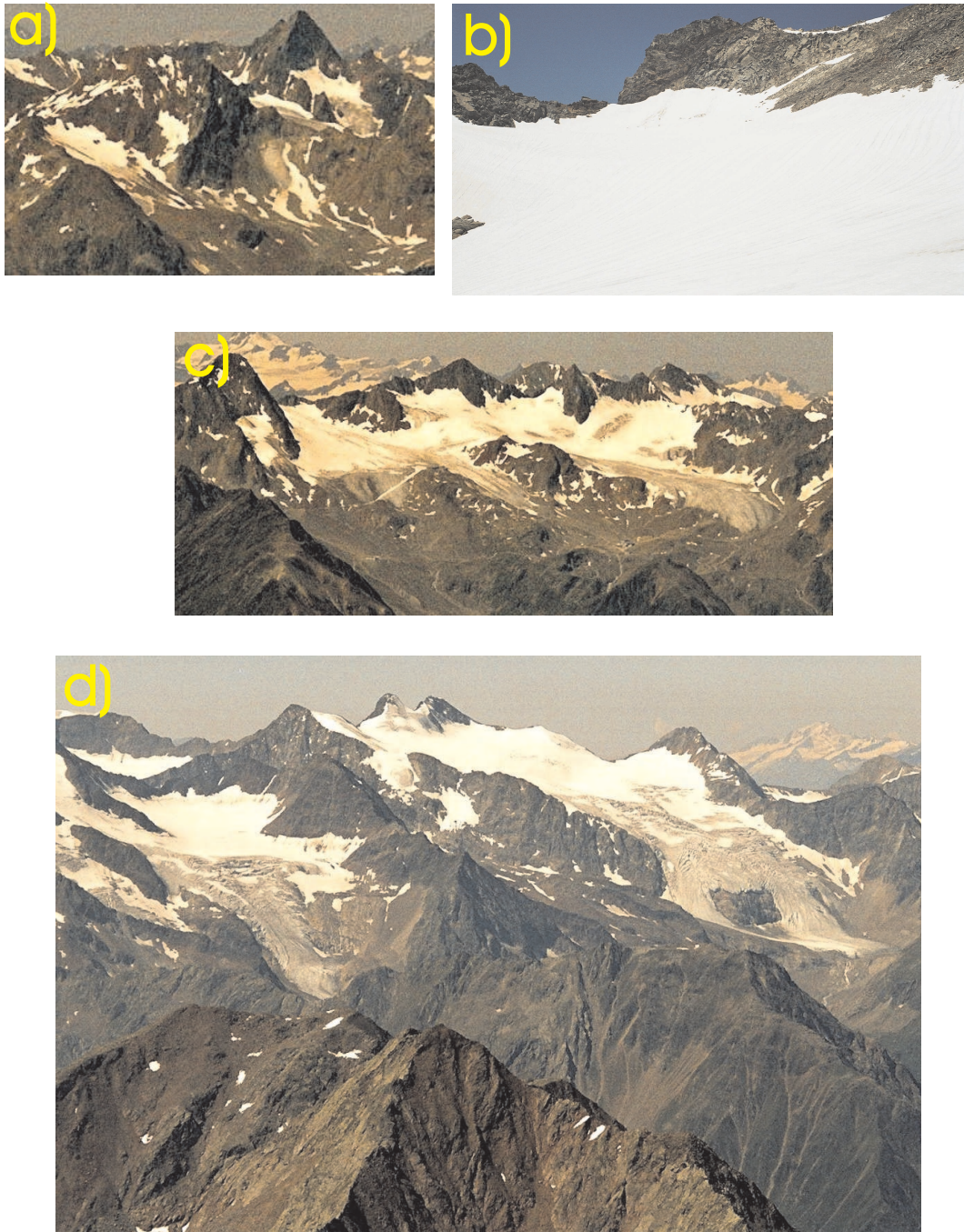


Figure 2.2: a) Daunkopf Ferner, b) Habicht Ferner, c) Daunkogel Ferner and Schaufel Ferner, d) Sulzenauferner on the right side of the image and a part of the Grünau Ferner on the left side of the image (photographed in July 2005 by the author).



Figure 2.3a shows the a part in the firn area of Grenzgletscher located in the Monte Rosa group. The layers of several years and decades are well visible in this picture. Figure 2.3b shows the Zwillingsgletscher and its crevasses with soot and dust layers. Figure 2.3c shows part of the glacier tongue of the Gornergratgletscher with a glacial river and 3 surface moraines. 2.3d shows the Eisferner located in the Ötztaler Alps. 2.3e is part of the tongue of the Briksdalbreen, an outflow glacier of Jostedalbreen in Norway, with soot and dust. 2.3f shows the Briksdalbreen outflow glacier with the lake into which the glacier calves.

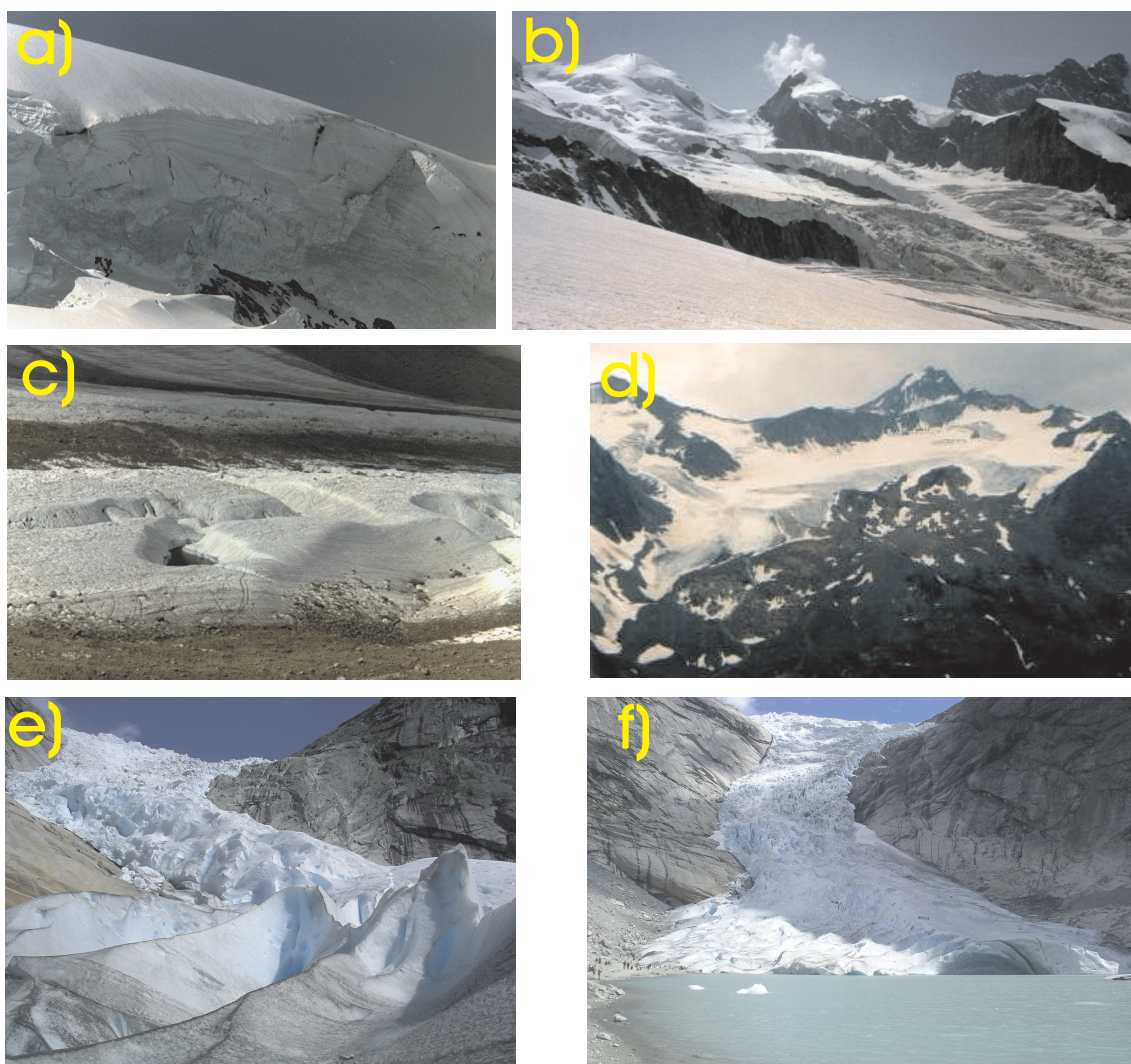


Figure 2.3: a) Grenzgletscher, b) Zwillingsgletscher, c) part of Gornergratgletscher, d) Eisferner, e) dust and soot at the tongue of the Briksdalbreenglacier, and f) tongue of the Briksdalbreenglacier (images a) to d) by the author, e) and f) by Wilma Onderwater).

## Glacier Zones

Glaciers can be divided into two areas, the accumulation area and the ablation area. The superimposed ice zone (SIZ) and the different snow zones (dry-snow zone, percolation zone and wet-snow zone) belong to the accumulation area. The bare ice zone and the firn layers (névé) from previous years belong to the ablation area. These two areas are divided by the equilibrium line (EL), where the ablation equals the accumulation.

Cold firn and ice can be found in the Alps in the upper reaches of several glaciers in the western Alps. Ice core drilling for studying past climate is feasible there, e.g. Colle Gnifetti in the Swiss Alps located between Zumsteinspitze and Signalkuppe (Schwikowski et al., 2005).

In figure 2.4 a schematic profile of the different zones in the accumulation area of a glacier is shown.

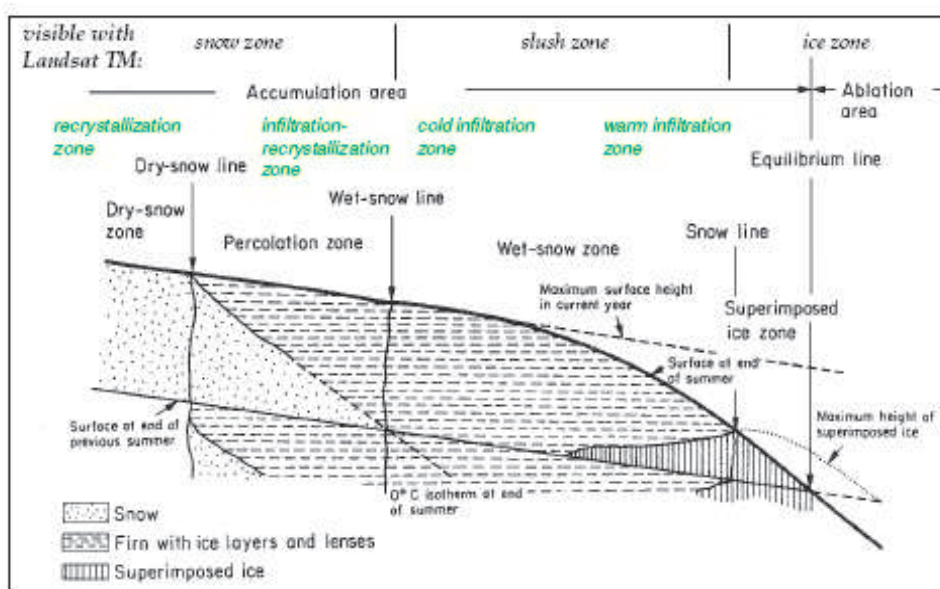


Figure 2.4: Schematic profile of the different zones in the accumulation area of a glacier; zones for mid-latitude glaciers in green (from Paul, 2003).

### 2.2.2 Mass Balance

Glaciers are influenced by the climate and its changes and show their reactions in changing mass and volume.

The mass balance of a glacier describes the change of glacier mass in space and time. It consists of the accumulation and the ablation. The accumulation includes mass

contributions by avalanches, freezing of rain, snow fall and all other processes that add material to the glacier. The ablation includes all processes which cause loss of ice and snow of a glacier, e.g. surface and bottom melt, evaporation and calving of icebergs. The specific mass balance  $b$  can be defined as change in mass per unit area and time and may be separated in winter balance  $b_w$  and summer balance  $b_s$ . The accumulation rate  $\dot{c}$  at a given point and given time is the increase of mass per unit area, often expressed as water equivalent. The ablation rate  $\dot{a}$  is the decrease of mass per unit area. The time integrals starting with  $t_1$  are called accumulation  $c$  and the ablation  $a$ . The total accumulation  $c_t$  and the total ablation  $a_t$  are integrated from  $t_1$  and  $t_2$ . The sum of summer ablation  $a_s$  and winter ablation  $a_w$  is can be expressed as the total ablation  $a_t$ . The following two equations are from Paterson (Paterson, 1994):

$$b = c + a = \int_{t_1}^t (\dot{c} + \dot{a}) dt \quad (2.1)$$

$$b_n = b_w + b_s = c_t + a_t = c_w + a_w + c_s + a_s = \int_{t_1}^{t_m} (\dot{c} + \dot{a}) dt + \int_{t_m}^{t_2} (\dot{c} + \dot{a}) dt \quad (2.2)$$

The terms  $t_1$  to  $t_m$  encompass the winter season and the terms  $t_m$  to  $t_2$  are summer season. Figure 2.5 shows the definition of the mass balance terms.

There are three common ways of mass balance determination. The glaciological method, the hydrological method and the photogrammetric method.

The glaciological method is not only time consuming in measuring the accumulation and ablation but also expensive. The accumulation is measured at the end of the accumulation period in snow pits. The height and the density of the snow of the last accumulation period is determined. Optionally also the snow morphology and the snow temperature are determined. The results of these measurements are the annual net accumulation  $b_a$ . The balance  $b_a$  of the snow pits in the accumulation area is than extrapolated to the whole area.

The ablation is usually measured using wooden, white painted stakes. On alpine glaciers the stakes are usually anchored in the glacier ice 8 to 12 metres deep. The melt losses in the ablation area are determined through the height changes of the stakes.

The hydrological method requires knowledge of the total precipitation of the basin (P), the run - off (R) and the loss of ice and snow by evaporation (E). The

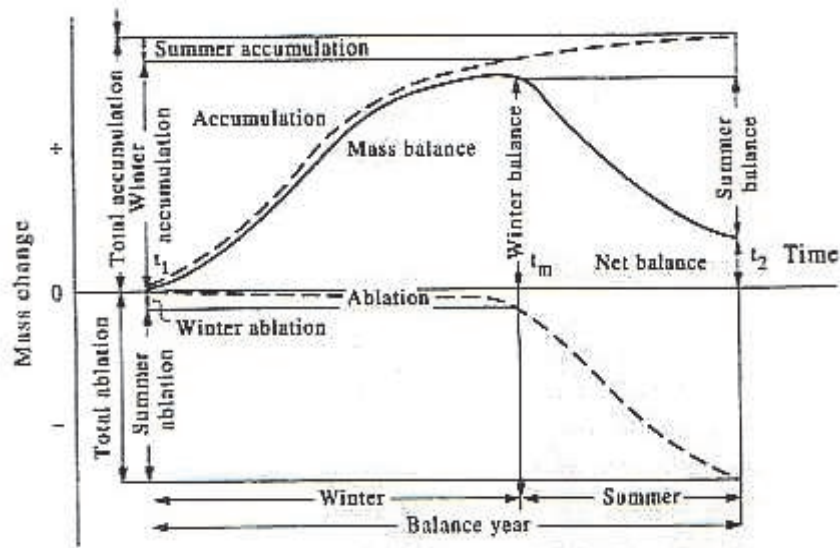


Figure 2.5: Definition of the mass balance terms (from Paterson, 1994)

difficulties of this method is the accurate determination of the evaporation and of the precipitation. The net balance is calculated using following equation (from Paterson, 1994):

$$B_n = P - R - E \quad (2.3)$$

A disadvantage of this method is that usually a basin contains more than one glacier so  $B_n$  of all glaciers and all snow patches in the area is measured, and the errors in  $P$  and  $E$  of the ice free surface increase the error of  $B_n$ .

The photogrammetric method uses exact topographic maps in intervals of one or more years to determine the changes in glacier topography. The volume of the glaciers are measured with this methods and can be converted into the mass change of the glaciers using average densities for firn and ice. The photographs have to be made at the end of the ablation period to get the best results in area changes.

The photogrammetric method provides data for glacier in areas where direct measurements cannot be made. It is also possible to obtain accurate topographic maps of glaciers by airborne laser scanning and radar interferometry.

## 2.3 The Use of Remote Sensing in Glacier Mapping

A main advantage in using space borne remote sensing data for glacier monitoring is the coverage of large area. This enables the scientists to monitor all glaciers of an extended area at the same time. Another advantage is the possibility of frequent repeat observations. Moreover, some of the new sensors have stereo capability enabling the retrieval of digital elevation models (DEM). Multispectral data enable automatic glacier classification using the spectral properties of snow and ice.

Problems result from cloudiness, because the acquisition time depends on the satellite orbit. Also shadowed and debris covered parts of the glaciers can cause problems in classifying.

### 2.3.1 Optical Properties of Ice and Snow

As described before the spectral properties of snow and ice are of relevance for multi-spectral classification of glaciers. In the visible part of the spectrum the reflectance of snow depends on pollutants (e.g. soot) but not on the grain size. In the near-infrared the reflection of snow and ice depends on the grain size whereas the dependence on pollution decreases. In addition, the spectral reflection of snow depends on the surface roughness and to a very small part on the liquid water content.

In the Landsat 5 TM bands TM1 - TM4 ( $0.45 \mu\text{m}$  -  $0.9 \mu\text{m}$ ) and the ASTER bands A1 - A3 the reflectance of snow is very high. Ice is darker in the visible part of the spectrum and also in the near infrared ice has a lower reflectance. In the short wave infrared, TM5 and TM7 and ASTER A4 - A5, the reflection of snow is very low and strongly depends on the grain size which makes ice even lower in the reflection. In the near infrared the reflection decreases with growing grain size and increasing wave length. The reflection of liquid cloud particles is very high also in the short wave infrared between  $1.6 \mu\text{m}$  and  $1.8 \mu\text{m}$ . This enables separate classification of clouds in the images because of their high reflection. Problems occur in both sensors with snow in shadow of e.g. clouds or mountain ridges and also with ice clouds.

Figure 2.6a shows the reflection of snow for various grain sizes for the Landsat 5 TM bands. Figure 2.6b shows the reflection of different types of snow and ice of a glacier after in situ measurements.

Figure 2.7 shows the model calculation by Wiscombe and Warren (Wiscombe and Warren, 1980) for the spectral reflectivity of snow in relation to the grain size. It clearly indicates the dependence of the reflectance on the grain size. In the visible part of the spectrum the albedo is not very sensitive to grain size, whereas in the



infrared part of the spectrum the albedo is sensitive to it. This difference between the VNIR and the SWIR can be used for calculation of the Normalised Difference Snow Index (NDSI, see 4.1.4).

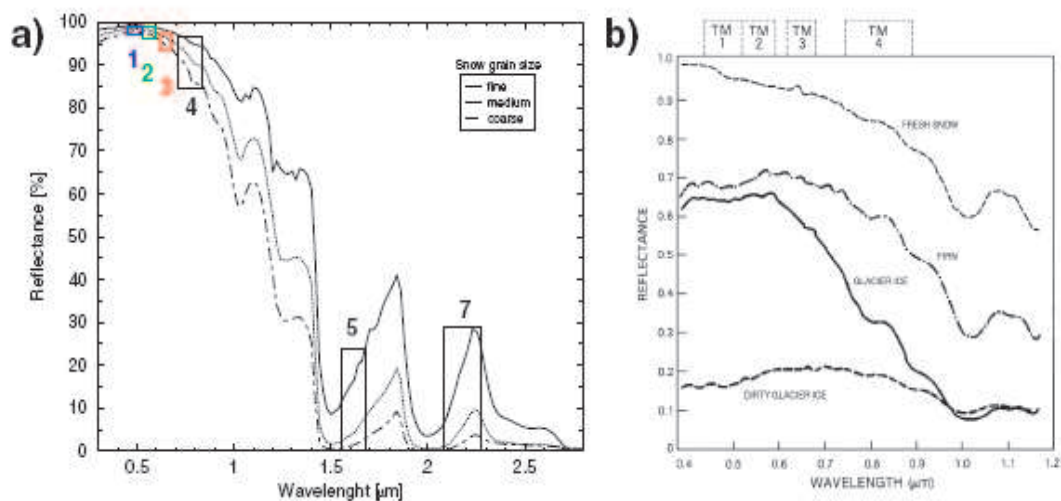


Figure 2.6: a) Reflection of snow for different grain sizes with the position of the spectral TM bands (from JPL, 2005). b) Reflectance curves for different glacier facies (from Hall et al., 1989).

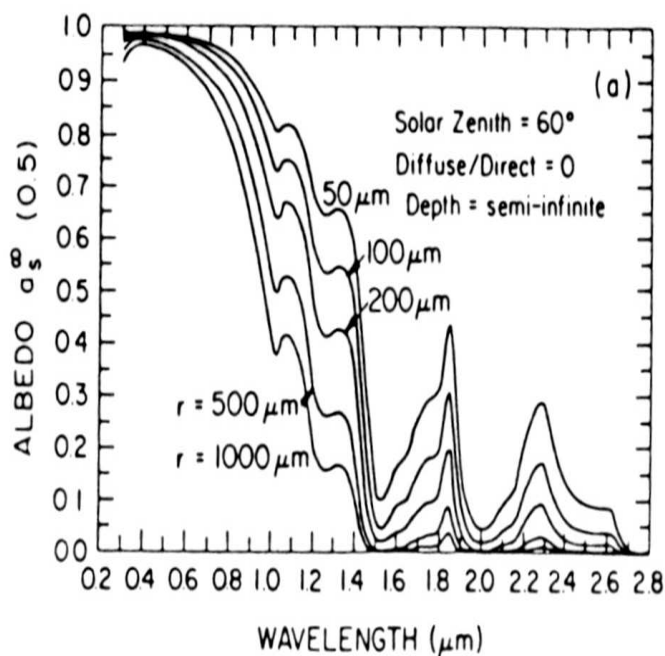


Figure 2.7: Spectral reflectivity in dependence of the grain size (from Wiscombe and Warren, 1980).



# Chapter 3

## Database

### 3.1 Satellite Data

In the past several studies on Austrian glaciers have been carried out using remote sensing. Studies on the Tyrolean glaciers using Landsat data, are reported by Paul (Paul, 1995), Paul (Paul, 2002D), Rott (Rott, 1976), Rott and Markl (Rott and Markl, 1989) and Hall et al. (Hall et al., 2003). Paul used Landsat 5 TM data to derive changes in the glacier area. Rott (Rott, 1976) used Landsat 1 MSS (and Landsat 2 MSS data) to analyse the snow cover of the central Tyrolean glaciers. Knap and Reijmer (Knap and Reijmer, 1998) and Greuell and de Ruyter de Wildt (Greuell and de Ruyter de Wildt, 1999) measured anisotropic reflection over melting glacier ice in the spectral range of Landsat TM bands. Nagler (Nagler, 1996) used Landsat TM data to classify snow and glaciers and to verify SAR data analysis. He calculated planetary albedo from the Landsat images and used different thresholds to derive glacier and snow maps.

In this thesis data of the two instruments, Landsat 5 TM and the ASTER instrument onboard of the Terra satellite, are used for monitoring the Stubai glaciers. The Landsat 5 TM satellite was launched on the 3<sup>rd</sup> of March in 1984 and carries the same instruments as the Landsat 4 TM satellite. The TM sensor of the Landsat 5 TM satellite is still working, while the MSS sensor data acquisition was suspended in 1992. Landsat 5 has a sunsynchronous orbit of 98.2° inclination. It crosses the equator at about 9:45 a.m. local time. The orbit height above the Earth's surface is 705 km. One orbit takes the satellite about 100 minutes. The TM band pixel size for the spectral bands 1 to 5 and the spectral band 7 is 30 meters by 30 meters. The pixel size for the spectral band 6 is 120 meters by 120 meters. The quantisation for all spectral bands of the Landsat 5 TM satellite is 8 bits. In table 3.1 the spectral range and the resolution of the Landsat 5 TM sensor are shown. Table 3.2 summarises

the actual status of the Landsat mission (USGS-EROS, visited October 2005).

A typical combination of the Landsat 5 TM channels for a False Colour Composite (FCC) image are the bands 4,3 and 2 or 5,4 and 3. With this combination water bodies appear dark blue to black, snow and clouds appear in white and vegetation appears in red.

Band	Wavelength( $\mu\text{m}$ )	Resolution(m)	Radiation
1	0.45-0.52	30	VIS
2	0.52-0.60	30	VIS
3	0.63-0.69	30	VIS
4	0.76-0.90	30	NIR
5	1.55-1.75	30	SWIR
6	10.40-12.50	120	TIR
7	2.08-2.35	30	SWIR

Table 3.1: Spectral range and resolution of the Landsat 5 TM spectral bands (modified after [http://eros.usgs.gov/guides/landsat\\_tm.html](http://eros.usgs.gov/guides/landsat_tm.html))

Satellite	Sensors	Launched	Decommissioned
Landsat1	MSS, RBV	23.7.1972	6.1.1978
Landsat2	MSS, RBV	22.1.1975	25.2.1982
Landsat3	MSS, RBV	5.3.1978	31.3.1983
Landsat4	TM, MSS(2)	6.7.1982	15.6.2001
Landsat5	TM, MSS(2)	1.3.1984	(1)
Landsat6	MSS, ETM	5.10.1993	lost at launch
Landsat7	ETM+	5.4.1999	SLC* failure 31.3.2003

Table 3.2: Status of Landsat satellites. (1)currently operational, (2)MSS data acquisition suspended in 1992. \*SLC= Scan Line Corrector (from [http://eros.usgs.gov/guides/landsat\\_tm.html](http://eros.usgs.gov/guides/landsat_tm.html))

The ASTER instrument is one of five instruments (ASTER, CERES, MODIS, MOPITT and MIRS) onboard the Terra satellite. Terra is the first of a series of satellites of the NASA's Earth Observing System (EOS). Terra was launched on the 18<sup>th</sup> of December in 1999. It has a sun-synchronous orbit of 705 km altitude. Inclination is 98.3 degrees from the Equator. The orbit period of the satellite takes 98.88 minutes. Terra crosses the Equator at 10:30 a.m. (north to south) and has a

repeat cycle of 16 days.

Because of the other instruments onboard the Terra satellite, ASTER does not collect data continuously. It is an on-demand instrument and collects an average of 8 minutes of data per orbit. Each ASTER scene covers an area of 60 km by 60 km. The ASTER instrument contains 3 subsystems (VNIR, SWIR and TIR) which are pointable in the crosstrack direction. These 3 subsystems operate in three visible and near-infrared (VNIR) channels, six shortwave infrared (SWIR) channels and five thermal infrared (TIR) channels. ASTER also provides stereo viewing capability for digital elevation model (DEM) creation (band 3N and 3B in table 3.3). The quantisation of the spectral bands 1 to 9 is 8 bits and for the spectral bands 10 to 14 is 12 bits. A list of the channels, their spatial resolution, wavelength and radiation is shown in table 3.3.

With the launch of Terra's sister satellite AQUA in May 2002, NASA started the second satellite of the EOS project. Like the Terra satellite, Aqua has a sun-synchronous orbit. Aqua crosses the Equator at 1:30 p.m. and Terra at 10:30 a.m.. This difference in the time crossing the Equator enables scientists to focus on different aspects (e.g. climate) and to see daily changes (e.g. clouds, water vapour) in the Earth's surface. In contrast to the Terra satellite Aqua does not have the sensor ASTER.

On 15<sup>th</sup> July 2004 the third component of the EOS project, Aura, was launched.

For both satellites the data can be ordered through the Earth Observing System Data Gateway (EDG), from the Japanese System GDS or from the USGS Global Visualisation Viewer (<http://glovis.usgs.gov/>) where the data also can be previewed.

Band	Wavelength( $\mu\text{m}$ )	Resolution(m)	Radiation
1	0.52-0.60	15	VIS
2	0.63-0.69	15	VIS
3N	0.78-0.86	15	NIR
3B	0.78-0.86	15	NIR
4	1.60-1.70	30	SWIR
5	2.145-2.185	30	SWIR
6	2.185-2.225	30	SWIR
7	2.235-2.285	30	SWIR
8	2.295-2.365	30	SWIR
9	2.360-2.430	30	SWIR
10	8.125-8.475	90	TIR
11	8.475-8.825	90	TIR
12	8.925-9.275	90	TIR
13	10.25-10.95	90	TIR
14	10.95-11.65	90	TIR

Table 3.3: Spectral range and resolution of the ASTER instrument spectral bands (N = nadir looking, B = backward looking).

To see changes in the glacier area of the Stubaier glaciers, Landsat 5 TM data from 1985 and ASTER data from 2003 were used.

The Landsat 5 TM data have a cloud cover of 0%. For the northern part of the Stubaital, the ASTER image has a cloud cover of 2% and for the southern part it has a cloud cover of 8%. In table 3.4 specifications of the used satellite images are listed.

Due to the cloud cover in the ASTER images it is not possible to analyse all glaciers in Stubaital. Especially in the southern part of Stubaital the clouds cover nearly half of the glaciated area. Figure 3.1 shows the area that both sensors, the ASTER sensor and the Landsat 5 TM sensor, cover.

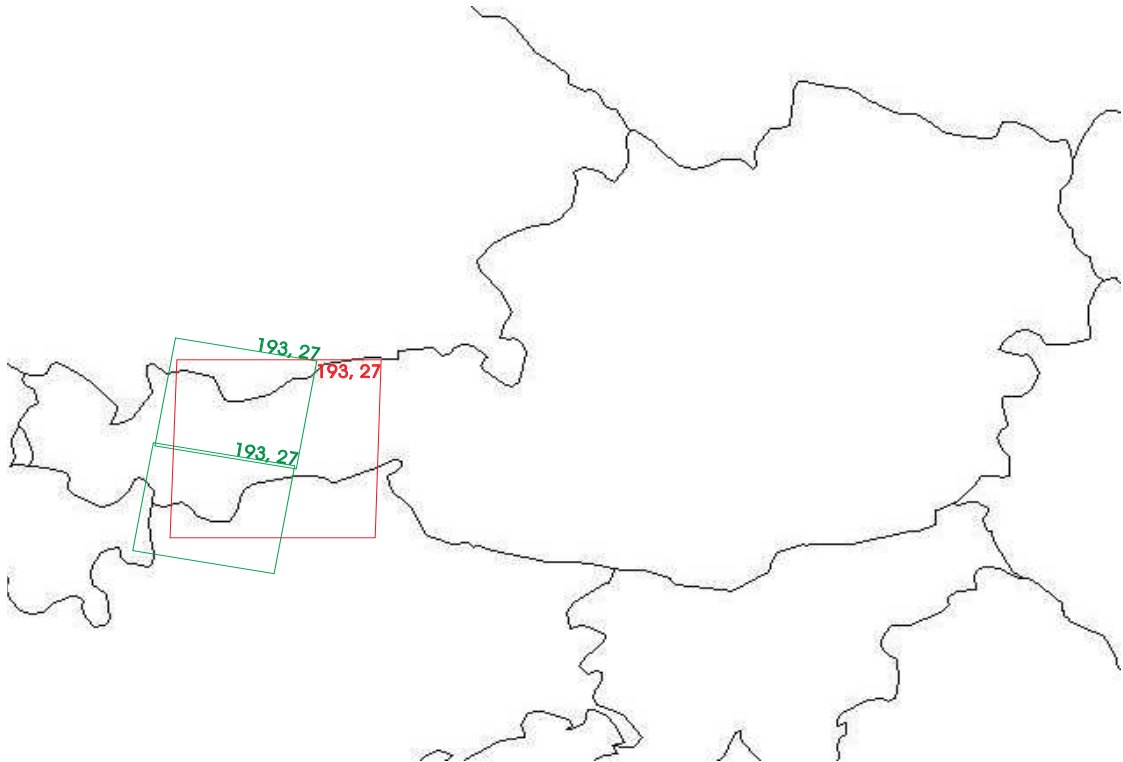


Figure 3.1: Outline of Austria with the position of the ASTER and Landsat 5 TM images. The green boxes show the position of the ASTER images, the red box shows the position of the Landsat 5 TM image used for this study.

Sensor	Path	Row	Date	Cloud Cover	Description
ASTER	193	27	2003-08-23	8%	southern part
ASTER	193	27	2003-08-23	2%	northern part
Landsat 5 TM	193	27	1985-09-30	0%	

Table 3.4: Information on the used satellite images.

## 3.2 Digital Elevation Model - DEM

An important information source of measuring glacier parameters are Digital Elevation Models (DEMs). Information on using DEMs in glacier research is given by Peipe et al. (Peipe et al., 1978) and Rentsch et al. (Rentsch et al., 1990). Berthier et al. (Berthier et al., 2004) used SPOT satellite images to calculate DEMs for thickness measurements of the "Mer de Glace" glacier in the Mont Blanc area.

DEM's can be obtained by photogrammetric analysis of a pair of stereo images of the same area. These stereo images can be generated by aerial photography, or stereo satellite images. Other options for DEM generation are laser scanning and radar interferometry.

The DEM used, `dem25_westoesterreich.pix`, has a raster size of 25m per 25m and a height resolution of 1m. It was used for orthorectification of the Landsat 5 TM and the ASTER data. For geocoding the satellite imagery a set of ground control points (GCP's) was derived using GCPWORKS of EASI/PACE (see Chapter 4). For geocoding the software SORTHO was used.

The DEM is important for glacier mapping to obtain watershed information enabling the separation of a glacier. To find these boundaries on glaciers the program WATERSHED analysis was used. An example in the Stubaital is the Lisenser Ferner, which is divided in two parts by the waterdivide. The main part is the Lisenser Ferner and the smaller part the Lisenser Ferner Berglas, which drains into another valley (see Chapter 4).

For obtaining the central flowlines of the glaciers a triangular irregular network (TIN), created by the DEM `dem25_westoesterreich.pix`, was used (Chapter 4).

The projection used is the Austrian "Bundesmeldenetz" BMN projection with the Datum Austria. It is based on the MGI (Militär Geographisches Institut) reference system with an, especially for Austria, optimised Bessel 1841 ellipsoid. In this optimised ellipsoid the deviation from the geoid varies between -2.5m to 3.5m whereas in the WGS84 it ranges from 43m to 52m.

In the Transverse Mercator Projection Austria is divided into 3 zones, M28 for the western part, M31 for the centre of Austria and M34 for the eastern part of Austria. According to this, Stubaital lies in the M28 zone. Table 3.5 shows the specifications for M28.

The georeferencing information in the satellite images and the DEM contains the Earth model, TM, the used ellipsoid, E002 [Bessel 1841], and the datum used, D501 MGI Hermannskogel [Austria].



Zone	Central Meridian	Scale	False Easting	False Northing
M28	10°20'	1	150 000m	-5 000 000m

Table 3.5: Specifications for TM zone M28

### 3.3 The Austrian Glacier Inventory

Austrian glaciers have been monitored since the early 19<sup>th</sup> century. The first inventory was compiled by E. Richter in 1888. With the fifth regional recording the glacier data became more accurate. Groß (Groß, 1987) mapped the ice covered area of 1850 (1011  $km^2$ ), 1920 (808  $km^2$ ) and 1969 (542  $km^2$ ) within the present Austrian borders. For the Stubaital the glaciated area in 1969 was 6077 ha.

The Austrian Glacier Inventory of 1969 was based on a special aerial photogrammetric survey. For some small glaciers the analysis had to be done using topographic maps in the scale of 1:25.000 and 1:50.000. The aerial photographs have a resolution of about 0.5 m. The photographs and contour maps have been analysed using photogrammetric and cartographic methods in a scale of 1:30.000.

The resulting maps contain glacier boundaries, snow lines, moraines, isolines and spot heights in a scale of 1:10.000 to 1:50.000. The height accuracy is about 1m (see Eder et al., 2000).

The new Austrian Glacier Inventory of 1997, based on aerial photographic surveys from 1996 to 1998 is still being processed. The image scale varies from 1:15.000 to 1:35.000. The aerial photographs have been digitised with a resolution of 15 $\mu$  and 30 $\mu$  using the photogrammetric precision scanner PS1 (Zeiss). Based on these images digital elevation models were produced using a semi-automatic photogrammetric method with a height accuracy of 1m (summary of comments by Astrid Lambrecht).

All glaciers of the inventory as well as moraines and lakes have been manually delineated.

The Austrian Glacier Inventory of 1969 has been digitised. For some parts of the inventory (e.g. Ötztal) the available maps could also be digitised. For some glaciers the aerial photographs had been analysed again. The analysis for the new inventory is carried out using GIS technology. Output from the production process includes the minimum, maximum and mean elevation of the glaciers, the total area, the area of the glaciers for individual elevation bands and also the difference between the two glacier surfaces from 1969 and 1997.

Figure 3.2 shows the aerial photograph of the new Austrian Glacier Inventory for

Alpeiner Ferner with the borders of 1969(blue), 1985 (Landsat 5 TM, green), 1997 (red) and 2003 (ASTER, magenta).

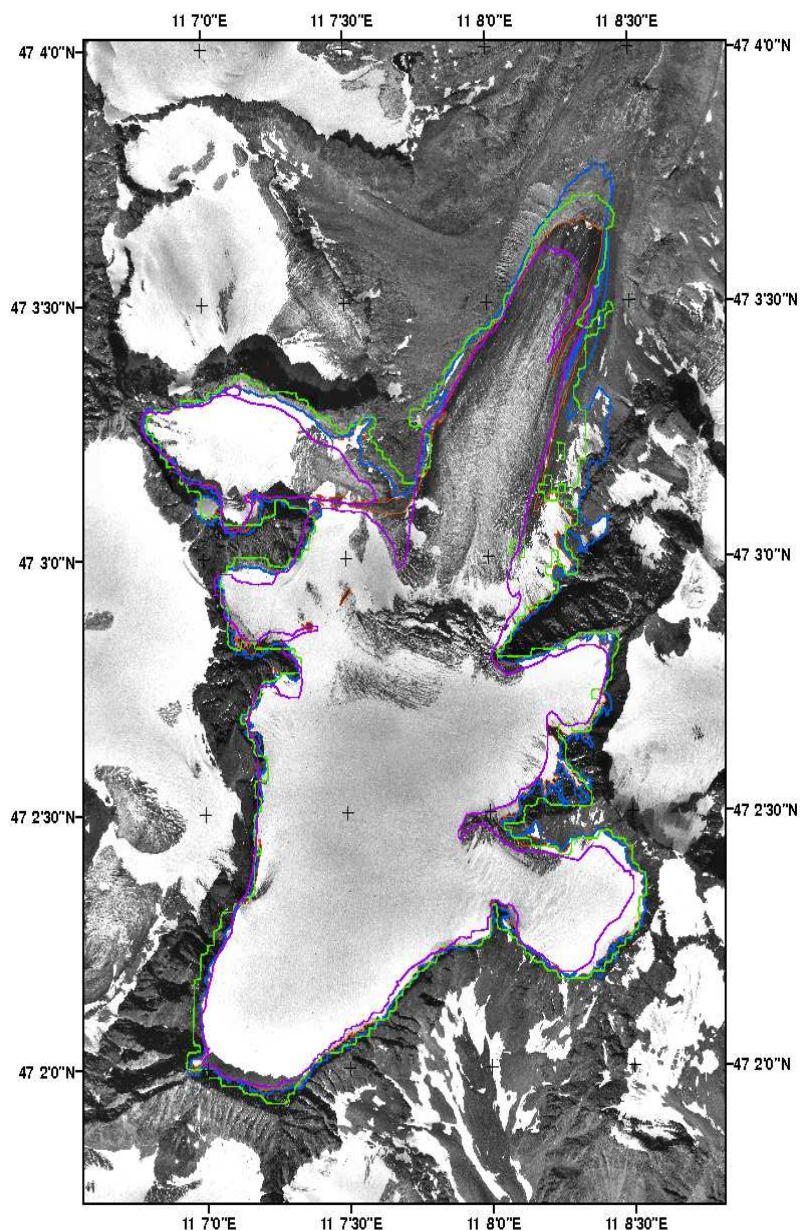


Figure 3.2: Aerial photograph of the new Austrian Glacier Inventory for Alpeiner Ferner with glacier boundaries from aerial photogrammetry (1969 = blue, 1997 = red), Landsat TM (1985 = green) and ASTER (2003 = magenta)

# Chapter 4

## Methods and Algorithms

### 4.1 Algorithms of the GLIMS - Project

In chapter 2 the data and algorithms of the GLIMS - project are discussed. In this chapter the methods used to obtain the GLIMS - specific metadata are described. The glacier used as test area for explaining the methods is the Alpeiner Ferner, located in the northern section of Stubaital.

As described in chapter 3 (see 3.1), the Landsat 5 TM and the ASTER sensor have slightly different bands. Table 4.1 shows the bands for the Landsat 5 TM and for the ASTER sensor used in this study.

TM Sensor	Landsat 5 TM / $\mu\text{m}$	ASTER / $\mu\text{m}$	ASTER Sensor
1 (blue)	0.45- 0.52	-	
2 (green)	0.52 - 0.60	0.52 - 0.60	1
3 (red)	0.63 - 0.69	0.63 - 0.69	2
4 (NIR)	0.76 - 0.90	0.78 - 0.86	3
5 (SWIR)	1.55 - 1.75	1.60 - 1.70	4
7 (SWIR)	2.08 - 2.35	2.145 - 2.43 <sup>1</sup>	5 - 9

Table 4.1: Spectral bandwidths in  $\mu\text{m}$  of the Landsat 5 TM sensor and the ASTER sensor.  
<sup>1</sup> =sum of band 5 to band 9 of the ASTER sensor.

Table 4.2 shows the spectral radiance  $L_{max,\lambda}/(\text{W}/\text{m}^2\text{sr}^1 \mu\text{m}^1)$  and the solar exoatmospheric spectral irradiance  $E_{sun}/(\text{W}/\text{m}^2 \mu\text{m}^1)$  for the Landsat 5 TM and the ASTER sensor. The values for the ASTER sensor of the spectral reflectance  $L_{max,\lambda}$  are values for normal gains settings. ASTER data has gain settings from high gain, normal gain, low gain 1 and low gain 2. The values for  $E_{sun}$  for the ASTER sensor are obtained from Smith, 2005 (Smith, 2005) from the middle col-

TM	$L_{max,\lambda}$ (W/m <sup>2</sup> sr <sup>1</sup> μm <sup>1</sup> )	$E_{sun}$ (W/m <sup>2</sup> μm <sup>1</sup> )	ASTER	$L_{max,\lambda}^{*1}$ (W/m <sup>2</sup> sr <sup>1</sup> μm <sup>1</sup> )	$E_{sun}^{*2}$ (W/m <sup>2</sup> μm <sup>1</sup> )
1	152.1	1957	-	-	-
2	296.81	1829	1	427	1847
3	204.3	1557	2	358	1553
4	206.2	1047	3	218	1118
5	27.19	219.3	4	55.0	232.5

Table 4.2: Spectral radiance  $L_{max,\lambda}/(W/m^2sr^1 \mu m^1)$  and solar exoatmospheric spectral irradiance  $E_{sun}/(W/m^2 \mu m^1)$  for Landsat 5 TM and ASTER. \*<sup>1</sup> = values for normal gain settings. \*<sup>2</sup> = values from the middle column in the article from Smith (Landsat 5 TM from: Chander, B. and B.Markham, 2003 and Epema, G.F., 1990; ASTER from: Smith, A.M.S., 2005).

umn (Thorne et al. (A)). The planetary albedo for each channel of the ASTER and Landsat 5 TM images was not calculated in this thesis. Because of the low gain settings in both ASTER images for the VNIR bands to much errors with the surrounding terrain arose.

The different band numbering of the 2 satellites shows that the ratio of the TM bands 4/5 for the ASTER sensor corresponds to the ratio of the ASTER bands 3/4. In the following sections each parameter referring the GLIMS - project for the Landsat 5 TM and for the ASTER sensor is described separately.

The description follows the enumeration of the **GLIMS Algorithm Working Group** (Kääb, 2004). The software used is described in Appendix A.

#### 4.1.1 Geolocation and Orthorectification

For analysing satellite imagery in GIS applications the data need to be in the same map projection. The geolocation process was used to transform Landsat 5 TM and ASTER row/column coordinates into earth based map projection. The used map projection in this thesis, TM E002, is described in chapter 3.2. Beside the transformation of the row and columns, elevation too, needs to be corrected especially in mountainous regions. The used DEM for terrain elevations was again the dem25\_westoessterreich.pix. Also a set of Ground Control Points (GCP's) is needed in the orthorectification process. The first step of the orthorectification of satellite images from both sensors was the extraction of the files. The ASTER files were extracted from the .hdf file using the "import to PCI" tool of the program GEOMAT-ICA. The data was stored in two files, one for the VNIR channels 1, 2, 3N, vnir.pix,

and one for the SWIR channels 4 and 5, `swir.pix`. With the module `PCIMOD` of the program `XPACE` two 8-bit channels were added to `vnir.pix` and with the module `REGPRO` the two channels of the `swir.pix` file were registered to the `vnir.pix` file. This file was renamed to `08232003dn.pix`. The next step for the ASTER file was to change the georeferencing settings from UTM, WGS84 into pixel because PCI is not able to transform from one reference geometry into another.

The Landsat 5 TM file was extracted using the module `CDLANDC` of the program `XPACE`. Here all 7 channels were extracted into one file called `850930_1.pix`.

The orthorectification was done with `GCPWORKS` to obtain the Ground Control Points (GCP's), using also a DEM and the orbit segment. As described in chapter 3 (see 3.2) the Earth model used is the Transverse Mercator projection with the Datum: MGI [D501], Ellipsoid: Bessel 1841 [E002]. For the southern ASTER image 25 GCP's and 5 check points were manually identified; for the northern ASTER image 16 GCP's and 5 check points. 18 GCP's and no check points were identified for the Landsat 5 TM image.

The following modules were used for further orthorectification: `SMODEL` to calculate the mathematic model, `CIM` to generate the file for the DEM, `PROTM` to set the georeference segment of the DEM, `REGPRO` to register the DEM to the area and projection of the orthorectified ASTER and Landsat 5 TM image and `SORTHO` to orthorectify the satellite image using the DEM and the mathematical model segment.

For the last step, `SORTHO`, new output files for the geocoded ASTER and LANDSAT 5 TM images were generated.

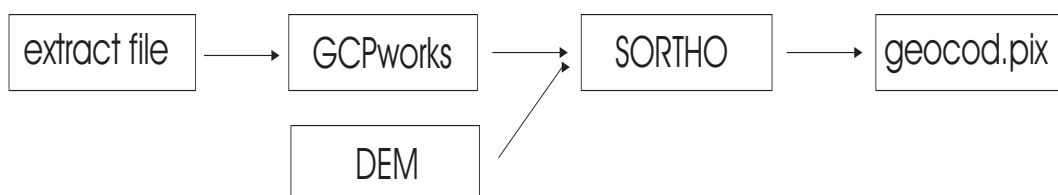


Figure 4.1: General workflow of orthorectification

### 4.1.2 Manual Mapping of Glacier Boundaries

The boundaries for the Stubai glaciers were mapped manually with the Vector Edit tool in the `imageworks` program. The first step was the creation of a new vector layer with the same georeferencing information as the ASTER and the Landsat 5 TM image. The boundaries are stored pixel by pixel (raster - based).

For the Landsat 5 TM image a false colour composit image (FCC) of the bands 543

with linear enhancement was used to delineate the boundaries. In the TM image of 30<sup>th</sup> September 1985 all glaciers except one, OE 16 NN, could be mapped. Glacier OE 16 NN is poorly visible in this image due to shadow from a mountain ridge.

For both ASTER images the FCC of the bands 432, also with linear enhancement, was used. In the northern part of the Stubaital only the Fotscher Ferner was masked by clouds in the ASTER image. Of the 88 glaciers located in northern Stubaital 5 glaciers were not visible in any of the bands of the ASTER sensor and could not be delineated. The glaciers in the southeastern part and the glaciers located at the Habicht peak were not visible due to clouds. In total, 29 glaciers were not visible due to clouds, 14 glaciers have disappeared or are completely debris covered.

The manual mapping of the glaciers boundaries for each ASTER image took about 3 days and for the Landsat 5 TM image about 5 days. The difficulties in manual glacier delineation resulted from shadow in some glacier parts, and from debris covered ice or rock and glaciers in the shadow of a mountain ridge. Figure 4.2 shows the area of Alpeiner Ferner, located in the centre of both images, with manually delineated glacier boundaries. In the ASTER image the glaciers on the right hand side lie in the shadows of clouds and therefore could not be mapped (see Appendix A).

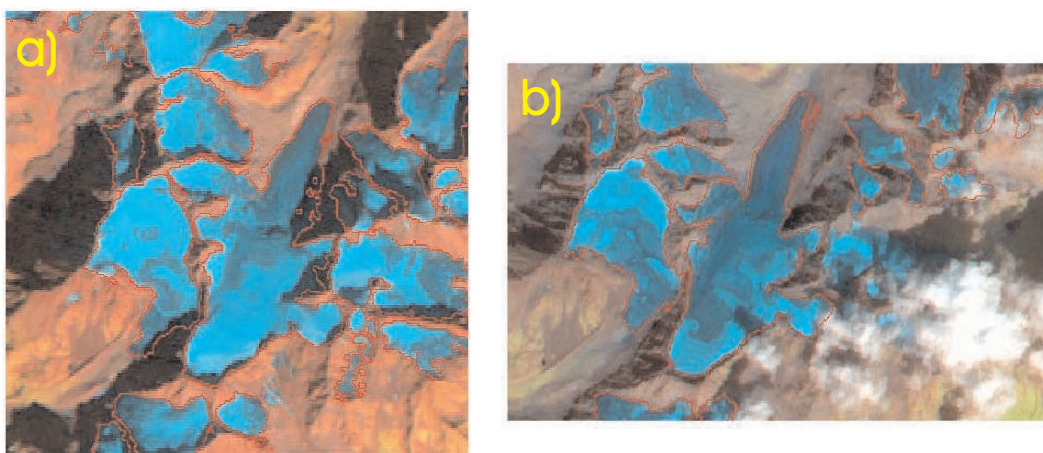


Figure 4.2: Manually mapped glacier boundaries for the area of Alpeiner Ferner in red, a) Landsat 5 TM, with root enhancement, b) ASTER southern part, with root enhancement.

The advantage of manual glacier delineation is the possibility to account for variations in solar illumination and surface albedo in contrast to automatic glacier mapping. Especially in the two ASTER images it was difficult to map the boundaries of some glaciers and even more difficult to find them in ratio images. Also for mapping the debris covered part of the glaciers manual delineation is probably the best solution. In the ASTER image the large debris covered part at the tongue of the Alpeiner Ferner is visible. Also on other glaciers large debris covered parts were

difficult to delineate.

### 4.1.3 Spectral Ratio

Snow and ice have high reflectance in the VNIR spectrum whereas at  $\lambda > 1.5\mu\text{m}$  they have very low reflection. So image ratioing of two spectral bands with different albedo for snow and ice enables segmentation of glaciers according to spectral properties.

The ratio of Landsat 5 TM band4/band5 reveals good results for glacier segmentation. For ASTER images the ratio to enhance glacier properties is band3 to band4. Values of planetary albedo for the Landsat 5 TM ratio image and the ASTER image have been calculated using following equations:

$$r_p = \frac{\pi L_{max,\lambda} d^2}{E_{sun,\lambda} \cos\theta_s} \quad (4.1)$$

$$r_{p,ratio} = \frac{L_{max,VNIR} E_{sun,SWIR}}{L_{max,SWIR} E_{sun,VNIR}} \quad (4.2)$$

Equation (4.1) is the equation for planetary albedo, equation (4.2) is the equation for the ratio images.  $L_{max,\lambda}$  is the spectral radiance in ( $\text{W}/\text{m}^2\text{sr}^1 \mu\text{m}^1$ ),  $E_{sun,\lambda}$  is the spectral irradiance.  $d^2$  is the Sun - Earth distance in AU and  $\cos\theta_s$  is the solar zenith angle. Planetary albedo of the Landsat 5 TM image ration is  $r_{p,TM} = 1.59$ . Planetary albedo of the ASTER image with low gain settings in the VNIR channels is  $r_{p,ASTER} = 1.1$ .

The results from both satellites are quite similar, both ratios enhance the spectral properties of snow and ice but have difficulties with the debris covered parts of the glaciers. Glaciers and snow have high DN's in the ratio images, terrain has very low DN's in the ratio images. Another difficulty is caused by dark lakes which might be classified as glaciers in the Landsat 5 TM band 5 and in the ASTER band 4. Figure 4.3a shows the ASTER ratio of the bands 3 and 4, figure 4.3b shows the Landsat 5 TM ratio of the channels 4 and 5. Difficulties with the debris covered parts and the difference in resolution between both satellites are evident. It also shows the problem with shadows in the Landsat 5 TM image e.g in the upper part of the Alpeiner Ferner.

To remove isolated pixels and gaps and to smoothen the glacier mask obtained from the ratio image, a 3x3 median filter was applied (see (Paul, 2003)). Figure 4.2c and figure 4.2d show the filtered ratio image of the ASTER and the Landsat 5 TM ratio

images. The difference between the unfiltered and the filtered images is clearly visible (see arrows). The 3x3 median filter also reveals a better glacier mask. Figures 4.2e and 4.2f show the difference between the unfiltered (green pixel) and the filtered (orange pixel) masks.

The used threshold to derive glacier masks was  $THR \geq DN 2.0$ , the planetary albedo has not been calculated in this thesis.

The resulting glacier areas were taken from the manual glacier boundary mapping results and not from the spectral ratio results. Especially the results for the ASTER images showed that debris and impurities on glacier surfaces could not be mapped with the spectral ratio.

#### 4.1.4 Snow classification by the NDSI -Normalised Difference Snow Index

The NDSI can be used to map snow covered area and also to detect snow and ice on a glacier. It is calculated by  $(100*TM2-100*TM5)/(TM2+TM5)$ . Values of a pixel at the boundary snow ice for TM 5: DN 8, TM 4: DN 111. The given values here are the spectral radiance at the sensor. Another way of getting a snow area mask is the use of the saturation component of the IHS colour-space transformation of the channels 5,4 and 3. The threshold  $THR \geq DN 80$  which is equivalent to an NDSI  $\geq 0.8$ , was derived empirically. It shows even better results than the simple ratio image. Again 3x3 median filter was used. Figure 4.4a shows the ratio for the NDSI, figure 4.4b shows the saturation component of the IHS-colour-space transformation. Figure 4.4c shows the area of the Alpeiner Ferner with the snow mask of the saturation component in magenta.

The ASTER image shows significant glacier retreat compared to the Landsat 5 TM image. Moreover, the snow shows that for many glaciers nearly no snow or firn covered part is left. In the Landsat image of 1985 in contrary the glaciers have substantial snow coverage.



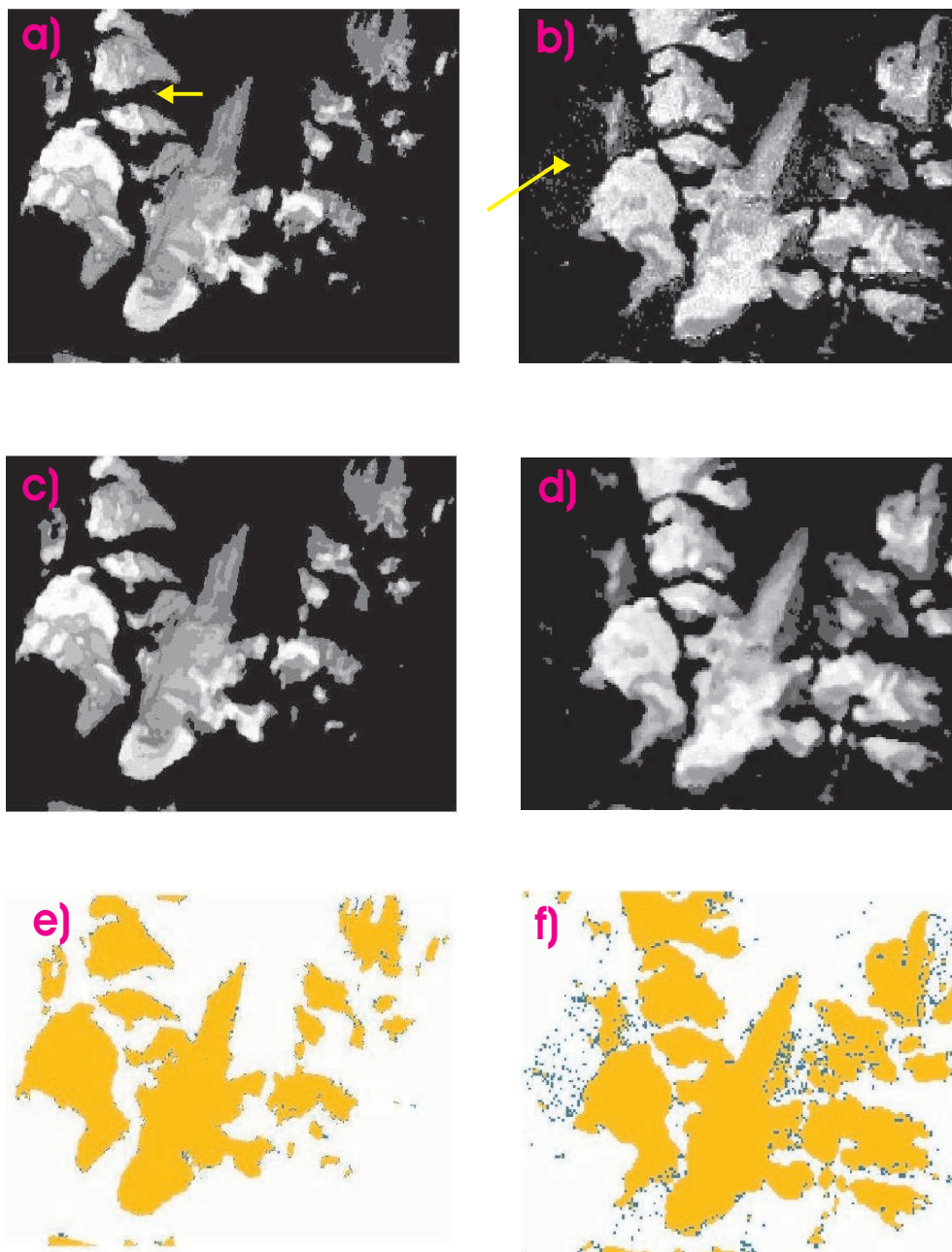


Figure 4.3: Ratio images a) Ratio A3/A4, b) Ratio TM4/TM5, c) filtered Ratio A3/A4, d) filtered Ratio TM4/TM5, e) and f) difference between unfiltered and filtered Ratio's

To monitor pro glacial lakes the Normalised Difference Water Index (NDWI) can be used. It is calculated using the Landsat channels 1 and 4 with the equation  $(100 \cdot TM1 - 100 \cdot TM4) / (TM1 + TM4)$ . For the ASTER image it is calculated using the equation  $(100 \cdot A2 - 100 \cdot A3) / (A2 + A3)$ . The factor 100 with which the channels are multiplied is used to obtain floating point numbers.

In the Landsat image of 1985 no glaciers had pro glacial lakes or had lakes dammed by moraines whereas in the ASTER of 2003 2 glaciers had lakes dammed by moraines.

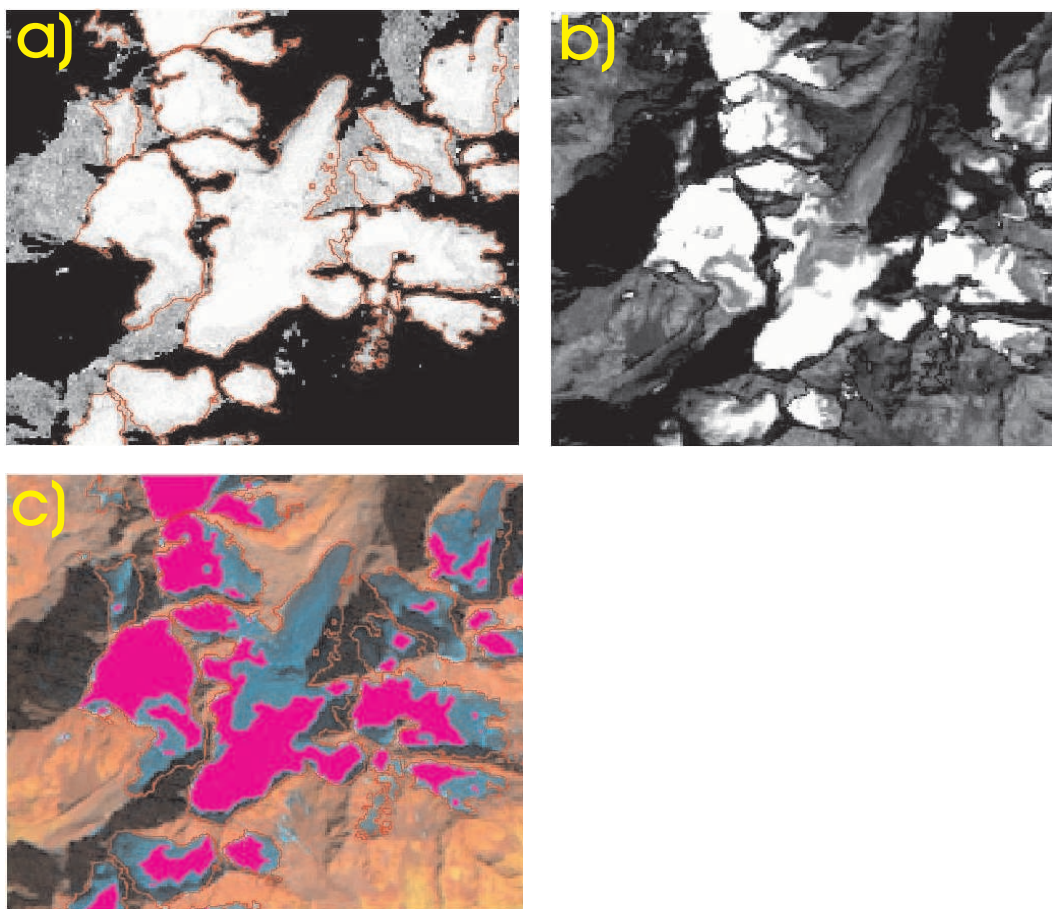


Figure 4.4: a) NDSI with the ratio  $(100 \cdot TM2 - 100 \cdot TM5) / (TM2 + TM5)$ , b) the saturation component of the IHS - colour - space transformation and c) the resulting snow mask in magenta obtained from the S543 component.

#### 4.1.5 Unsupervised Classification

The ISODATA clustering uses an algorithm to allocate each pixel into certain number of clusters, according to the pixels grayscale. In this thesis it is used to get an overview of glaciated areas. It is not used for further interpretation. ISODATA clustering uses a given number of image channels. The number of minimum clusters and maximum clusters, and the number of iterations need to be specified, for the other parameters the default values can be used.

The channels 1 - 5 have been chosen for the Landsat 5 TM image, channels 1 - 4 for the ASTER image. For both satellites ISOCLUS was carried out twice, one run with 20 classes and one run with 31 classes. The other parameters maxclus, minclus and maxiter remained the same. In both approaches the shadowed parts of the glaciers are not identified as separate class, but lumped with the class "rocks". For the other parts of the glaciers the best approach has to be chosen individually. In the

ASTER image the debris covered parts of the glaciers are classified as rock in both approaches. In the Landsat image the glacier parts in the shadow are classified as rock in both attempts (20 and 31 clusters). The creation of a glacier mask can be quite difficult especially for the debris covered parts and cloud shadows.

Figure 4.5a and 4.5b show the results for the Landsat 5 TM image for the whole research area for the classes with 20 clusters and 31 clusters.

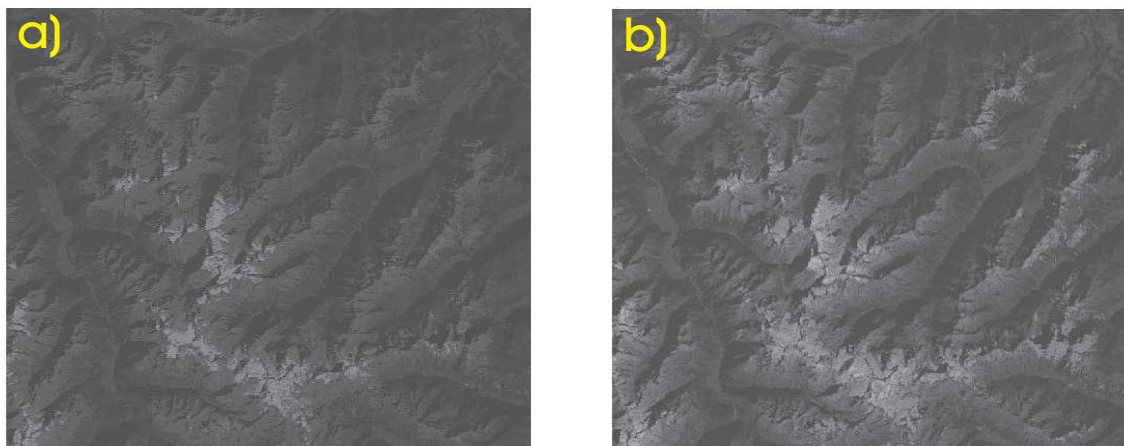


Figure 4.5: Unsupervised classification of the Landsat 5 TM image a) with 20 clusters, b) with 31 clusters.

#### 4.1.6 Supervised Classification

The supervised classification takes a little more time than the unsupervised classification because of the need of training areas. The first step in the supervised classification is the selection of training areas. These training areas should be carefully selected and accurate. They should also be distributed over the whole image. The 10 training areas in the Landsat image are: glacier tounge, water/lakes, towns, rock in sunlight, rock, rock/other in shadow, forest, snow on glacier, fields/grassland and clear ice. In the southern ASTER image 9 training areas were: bright snow, snow, ice/tounge area, water, fields, forrest, rock, clouds and an extra glacier class. In the northern ASTER image 10 training areas have been selected: ice, snow/firn, forest, fields, clouds, grassland, rock, town, water and shadow. Separate classes for different illuminations improved classification only in some parts of the images.

The next step was the generation of signatures of the training areas with the program CSG. After that, the program SIGSEP was used to calculate the separability between the signatures. This showed that for the Landsat image the class glacier tounge and clean ice were the pair with the minimum separability for the southern



ASTER image. The classes snow and the extra glacier class were the closest classes to each other. In the northern ASTER image the classes fields and grassland had the minimum separability. Figure 4.6 shows the results of the Maximum Likelihood Classification MLC for the northern ASTER image.

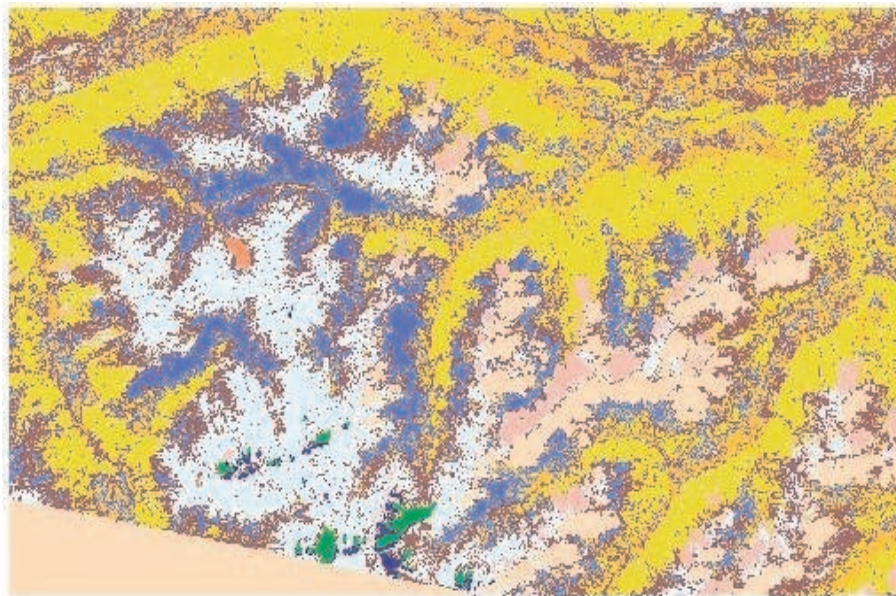


Figure 4.6: Maximum Likelihood Classification of the northern ASTER image. Classes: ice = green, snow/firn = dark blue, shadow = bright pink, clouds = flesh-coloured, town = red, rock = white, water = orange-pink, forest = yellow, fields = orange, grassland = blue.

#### 4.1.7 Debris

Debris and impurities on glacier surfaces can be of different composition, from small soot and dust particles to huge blocks of rock. Figure 4.7a shows the Ganjam Glacier, a glacier located at the Kailash in Tibet, with a tongue almost totally covered with debris. Figure 4.7b shows a part of the Vernagt Ferner, located in the Ötztal, with dust from the Sahara.

If a pixel on a glacier is dominated by debris and other material with low albedo and the exposed ice part is very small it appears in the spectral signal as rock. Thus it is classified as rock in the ratio  $TM4/TM5$ . Paul (Paul, 2003) used a  $TM4/TM5$  ratio image to obtain a black (= glacier) and white (= terrain) glacier mask and combined it with a vegetation free map obtained from the hue component of the IHS-colour-space transformation. The result was a mask with values assigned for glacier=0 and else=255. He then calculated the slope from the DEM and counted all slope

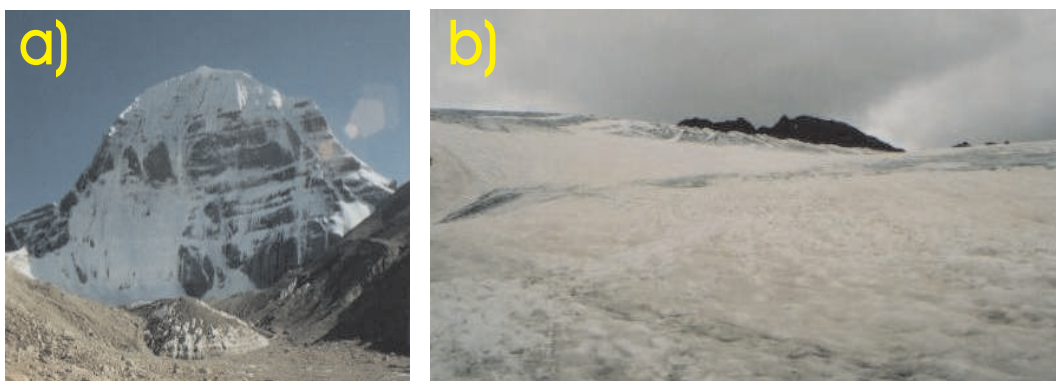


Figure 4.7: a) Debris covered tongue of a glacier located at the Kailash, b) Sahara sand at the Vernagt Ferner (a) photographed by the author in August 2004, b) photographed by the author in July 2004).

values below  $24^\circ$  with low albedo within the glaciated area as debris on glacier ice. The steeper, lower albedos were excluded from the glacier. Paul combined all three masks and produced a mask for debris. He then used the IPG module from PCI and a Fortran program to remove isolated "debris" pixels.

The approach for the ASTER image used in this thesis was accomplished by trial and error (see Appendix C). Because of the different spectral properties of ice and snow in the ASTER channels 3 and 4 the idea was, that a combination of both would create a mask with all needed information. A mask only with channel  $4 \leq DN26$  (no calculation of planetary albedo has been done in this thesis) delivers almost the same results as the combination of ASTER band  $3 \geq DN26$  and  $4 \leq DN26$ . With the use of channel 3, incorrectly classified pixel in the shadows can be removed so that the result of the combination is a mask which covers the whole glacier. A disadvantage of the debris mask for the ASTER image is that pixels in the shadow and pixels of cloud shadows have to be removed carefully.

Another approach for a debris mask is the use of the IHS transformation (see 4.2.1). For the ASTER images the Hue channel from the transformation of the channels 234 provides also a glacier mask with the debris covered area. The difference between both approaches is small so both can be used to create a debris mask. In this thesis the debris mask obtained from the hue component of the IHS transformation was used.

For Landsat 5 TM a different method was used. One problem in the Landsat image was that there was very little debris on the glaciers. To obtain a mask for the debris cover on the glaciers the hue component of the IHS-colour-space transformation (see Section 4.2) of the Landsat 5 TM channels 345 was used. The resulting mask was a total glacier mask including the debris covered parts and those parts which are

in the shadow. The later steps to get the debris mask where the same as in the ASTER image.

Figures 4.8a and 4.8b show the resulting masks for the ASTER and the Landsat 5 TM image. Beside the debris cover on the glacier tongues also the glacier parts in the shadow are classified.

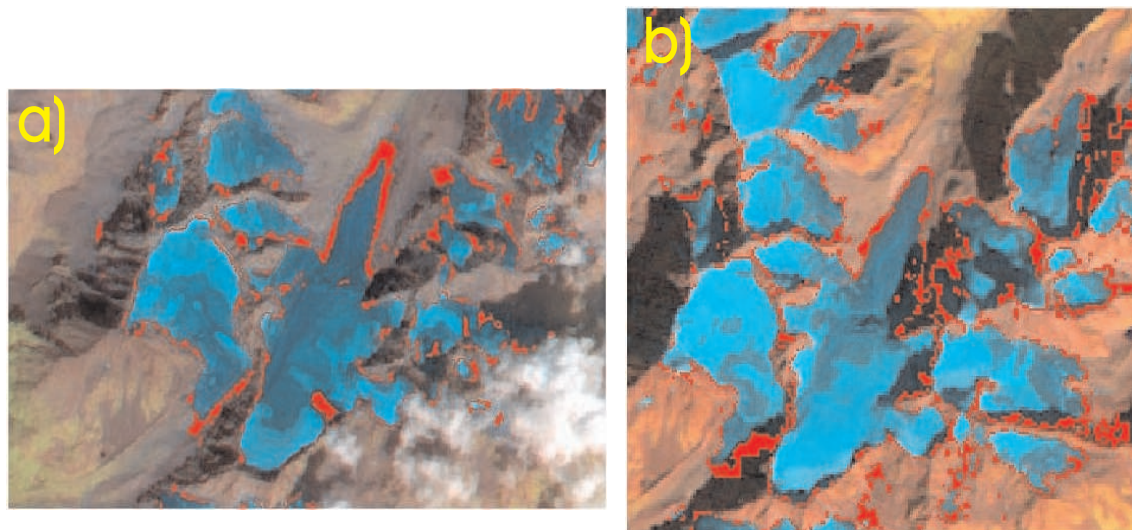


Figure 4.8: Resulting debris mask a) of the ASTER image in red, b) of the Landsat 5 TM image in red.

#### 4.1.8 Identification of Glacier Basins

The generation of glacier basins for the Stubai Glacier is important for the identification of ice divides, e.g. Lisenser Ferner and Lisenser Ferner Bergglas.

The basins are created using the modules DWCON, SEED and WTRSHED from PCI. A DEM is needed for this process.

With the first module the depressions are filled (FDEP), flow direction(FDIR), flow accumulation (FACCUM) and flow delta values(FDELTA) are calculated. With the module SEED the start cells at the outflow point are sought, a threshold is needed here. The module WTRSHED finds the watersheds using the results of SEED.

#### 4.1.9 Glacier ID - Points

In the Austrian Glacier Inventory of 1969 a point with lon/lat coordinates is stored for each glacier. These points were used to generate the glacier ID-points. A new .dbf file was created with the glacier ID and the name. The .dbf file was then loaded into ArcView and converted into an ESRI shapefile. The shapefile was then loaded

into imageworks to check the position of the ID points. 4 points had to be replaced due to the shrinking of the glaciers.

## 4.2 Other Algorithms used

Other algorithms have been used to get more information out of the ASTER and Landsat 5 TM images. As described in Section 4.1 the IHS-colour-space transformation was used to obtain the snow area on the glaciers and to obtain a debris mask. The PCA-Principle Component Analysis can be used to create a snow mask and also to enhance the difference between different kinds of snow, e.g. fresh snow and old snow.

### 4.2.1 IHS-colour-space Transformation

As described previously (see 4.1.7) an algorithm was needed to produce a glacier mask, which also includes the debris covered part of a glacier. The IHS transformation was used to convert the Landsat and ASTER channels into intensity, hue and saturation (IHS). The module uses two algorithms for transforming, the Cylinder and the Hexcone model. The model used here is the Cylinder model. In the Landsat image the channels 543 and in the ASTER image the channels 234 have been used. For both satellites the resulting images could be used to produce a snow mask from the saturation and the hue channel and to see the different types of snow in these channels. The hue channel of the ASTER images could be used to generate a glacier mask with the debris covered parts (see 4.1.7). In the Landsat 5 TM image the S345 and I345 channels are very similar to the TM4 and TM2 channels.

A problem in the Landsat image was the shadow at mountain slopes. In the ASTER image the cloud shadows caused misclassifications of glacier masks. Figure 4.9a shows the IHS composite from the ASTER image, 4.9b from the Landsat image. In the ASTER image the H234 glacier mask ( $\text{THR} \geq \text{DN } 80$ ) also classifies those glacier parts that are under the cloud shadows. Yet, lakes located in front of the glacier tongue are also classified as glacier and connected to the glacier. These pixels have to be removed from the final debris mask. In the Landsat image small mountain ridges between two glaciers are also classified as glacier. Here again manual correction is required.

Figure 4.10a shows the H234 component of the ASTER image, figure 4.10b the glacier mask obtained from the H234 component ( $\text{THR} \geq \text{DN } 80$ ), 4.10c the glacier mask from the ratio  $A3/A4$  and 4.10d the resulting debris mask calculated from the ratio mask minus the H234 mask. The arrow indicates the lake in front of the tongue



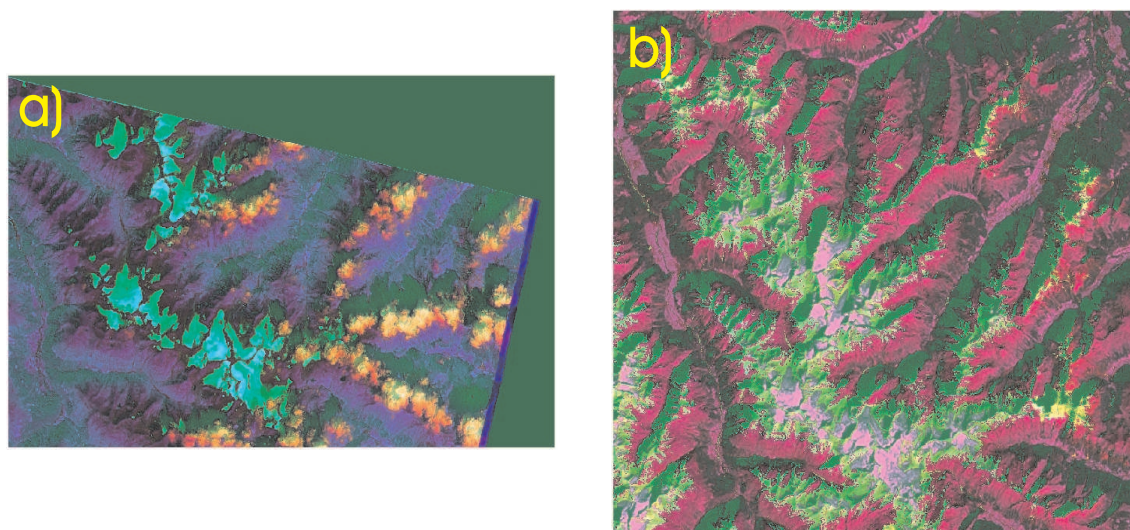


Figure 4.9: IHS-colour-space transformation composite of a) the ASTER 234 channels and b) the Landsat 345 channels

of Bachfallen Ferner.

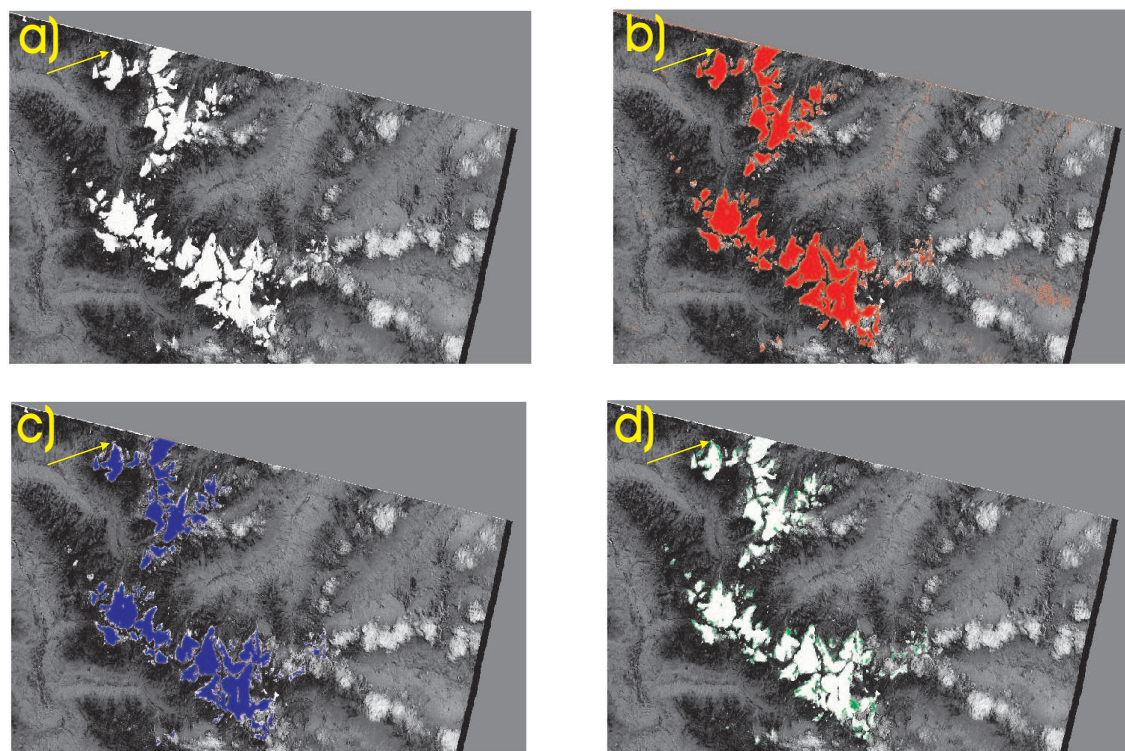


Figure 4.10: Illustration for generating a debris mask for the ASTER image obtained from the Hue component of the channels 2,3,4. a) Hue component, b) glacier mask, c) glacier mask obtained from the ratio  $A3/A4$  and d) the resulting debris mask.



### 4.2.2 PCA-Principal Component Analysis

PCA is a module of PCI that reduces the dimension of the input channels to obtain as much variance as possible in a small number of image channels (Richards, 2005). The new resulting uncorrelated channels are orthogonal to each other. The workflow for the computation of the PCs is first to calculate the covariance matrix, then the calculation of the eigenchannels and eigenvalues and finally the calculation of the PCs. The first PC, the eigenvector  $E_{ji}$ , is:

$$PC1 = \sum DN_1 \cdot E_{1i} \quad (4.3)$$

Sidjak and Wheate (Sidjak and Wheate, 1999) used PCA for snow cover mapping on the Illecillewaet glacier. In the Landsat image PC4 shows the snow and firn covered glacier areas whereas PC2 clearly isolates the glaciers from the surrounding terrain. In the ASTER image PC2 the glacier area and the clouds have very high DN's and cannot be separated. PC3 has very low DN's over glaciers and does not enable separation of rock and moraines and with debris covered ice. Figure 4.10a and 4.10b show PC2 and PC3 of the ASTER image. Figure 4.10c and 4.10d show PC2 and PC4 of the Landsat 5 TM image. The PC3 of the ASTER image as well as the PC4 of the Landsat image can be used for creating a snow mask for the glaciers as an alternative to the NDSI ratios.

### 4.2.3 Central Flowlines

In the Austrian Glacier Inventory of 1969 and 1997 the central flowlines were not derived. In this thesis the central flowlines were derived to see the approximate direction of the ice flows. Central flowlines were made for those glaciers which have a clearly identified tongue.

The delineation of the central flowlines was carried out using the program ArcView. A DEM is needed. The DEM was converted into a dem.grd file, loaded into ArcView and converted into a TIN, Triangular Network (see chapter 3.2). The central flowlines were created using the extension Spatial Analyst and the tool Steepest Path. The accuracy of these flowlines depends on the accuracy of the used DEM and can differ from the true central flowlines if a DEM is noisy.

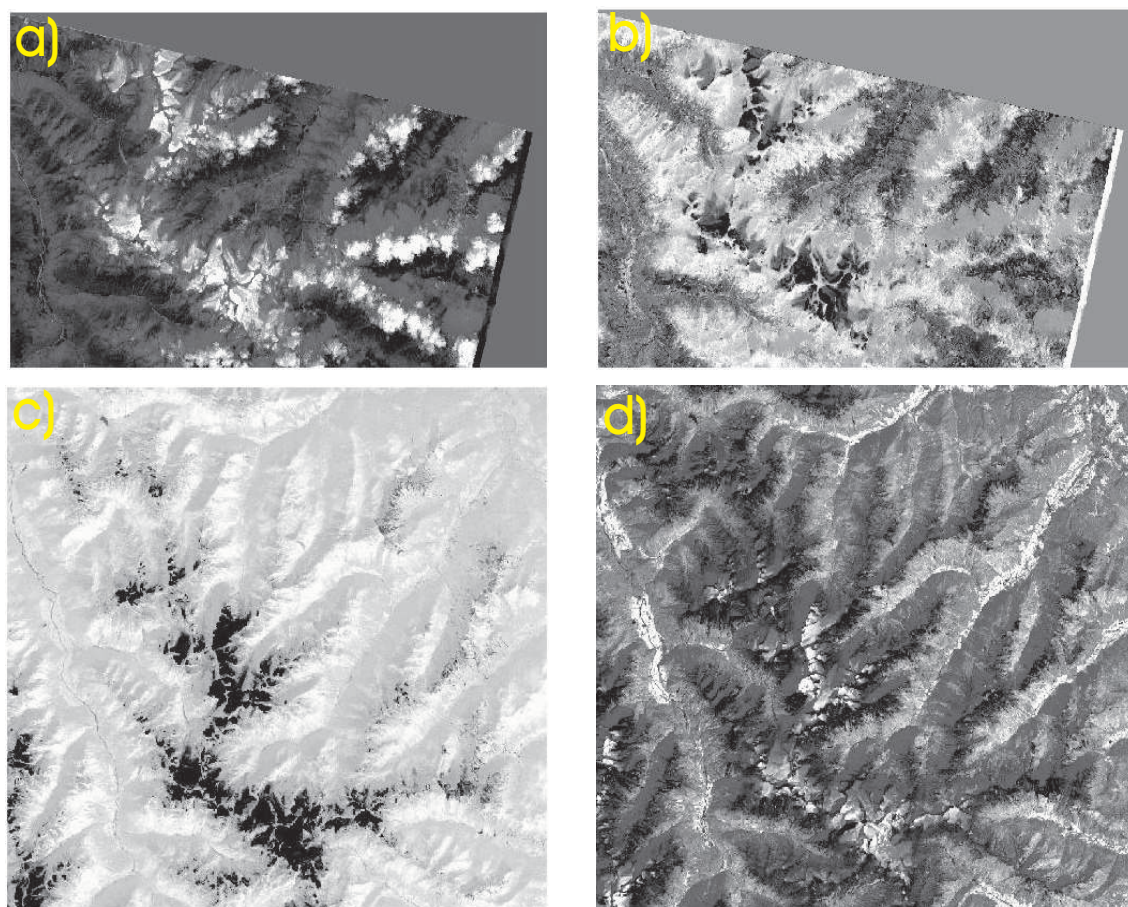


Figure 4.11: a) PCA2 and b) PCA3 of the ASTER image, c) PCA2 and d) PCA4 for the Landsat 5 TM image.

### 4.3 Summary on Methods used

In the bottom line not all of the previously mentioned methods were used in analysing glacier size. Geolocation and orthorectification had to be used to transform the satellite row/column coordinates into earth-based map projection. Manual mapping of glacier boundaries was used to obtain from ratio images independent glacier sizes. The results of this was used to write glacier attributes (e.g. ID, size) into the attribute file of the glacier boundaries file.

The NDSI ratio images were used in deriving snow covered areas on glaciers for the Landsat image. For deriving masks of snow covered areas the IHS transformation was used. The ratio images have not been used to derive glacier areas.

The two algorithms mentioned previously of deriving debris and impurities on glaciers surfaces are used for the GLIMS database.

Identification of glacier basins was important for the identification of ice divides and used to divide several glaciers, e.g. Lisenser Ferner and Lisenser Ferner Berglas.

The glacier ID points are used for the GLIMS database.

As mentioned previously the IHS transformation was used to identify debris and impurities of glacier surfaces and to generate snow masks for the glaciers.



# Chapter 5

## Results

### 5.1 Comments on Glacier Identification

The resulting glacier areas for the ASTER and the Landsat 5 TM sensors are quoted in Appendix B. Their percentage of change between 1985 and 2003 are also noted in Appendix B. The change of area between 1985 and 2003 uses the area of 1985 as a baseline. It also refers to those glaciers which are clearly identified in their whole area and are not obscured by clouds or shadows (see table B 3). Glaciers which disappeared in the ASTER image are listed in the tables (see table B 2). The glacier OE 16 NN is not included here because of too much shadow in the Landsat 5 TM image and in the ASTER image.

The glacier names were taken from the Austrian Glacier Inventory and for those glaciers with no names their number and NN are used for identification. Several glaciers are split into 2 or more parts. Difficulties occurred with glaciers which have a common ice divide. In addition some glaciers split into several parts which cannot be clearly assigned to a certain glacier. For those glaciers the digital Austrian Glacier Inventory of 1997 was used to allocate smaller glacier parts to their original glaciers. To divide glaciers at the ice divide, the glacier basin was used (see 2.1.8).

For the comparison with the Austrian Glacier Inventory of 1969 the classification of glaciers according to their class refers for both datasets to the class the single glaciers had in the Austrian Glacier Inventory of 1969. For the comparison with the Austrian Glacier Inventory of 1997 the classification of glaciers according to their class refers for both datasets to the class the single glaciers had in the Austrian Glacier Inventory of 1997.

## 5.2 Analysis of Results

### 5.2.1 Statistics of Glacier Size and Area at Given Dates

The Landsat 5 TM image of 30 September 1985 shows the whole glacier area of the Stubai Alps. With exception of one glacier, OE 16 NN, all glaciers are visible and could be classified. The manually derived boundaries of the glaciers include the debris covered ice. The automatically derived outlines exclude for some glaciers debris covered pixels or pixels in the shadow (see chapter 4.3). Glacier sizes derived from manual glacier boundary mapping were used. These debris covered pixel often cover only the area of one pixel and changes in area caused by them are small. In the Landsat 5 TM image very little debris covered ice is evident.

The areas of the glaciers include also the small debris covered parts. Table 5.1 shows the four glacier area classes used for grouping the Stubaital glaciers.

Class/km <sup>2</sup>	Number	Area/km <sup>2</sup>	Area/%
<0.1	19	1.14	1.83
0.1 to <0.5	63	13.81	22.17
0.5 to <1.0	20	14.42	23.15
1.0 to <5.0	14	32.91	52.84
<b>Total</b>	116	62.28	100

Table 5.1: Statistics of the 1985 image for the 4 area classes. The area columns list the whole area and percentage of all glaciers in the area classes, referring to the 1985 areas.

Table 5.1 displays in the area column the area which is covered by each class. The largest glacier in class 1 is Winnebach Ferner M with 0.095 km<sup>2</sup> and in class 2 it is Windacher Ferner with 0.432 km<sup>2</sup>. In class 3 the largest is Östlicher Grübl Ferner with 0.966 km<sup>2</sup> and in class 4 it is Sulzenau Ferner with 4.87 km<sup>2</sup>. Table 5.1 also includes the percentage of the total area of the single classes. Problems in analysing glacier size occurred with splitting up some glaciers into two or more parts. For some glaciers, e.g. Daunkogel Ferner and Schaufel Ferner, it was not clear to which of the glaciers the split off parts belong. As mentioned before, the Austrian Glacier Inventory shapefiles were used in these cases.

Manually derived boundaries are used for calculation of glacier size because of their accuracy compared to automatic derived outlines. The total size in the measured area in the 1985 Landsat image is 62.28 km<sup>2</sup>.

In the ASTER images 29 glaciers of the 117 glaciers located in Stubaital could not be mapped due to clouds and cast shadow. Of the remaining 88 glaciers 14

small glaciers have disappeared between 1969 and 2003. Mapping glaciers in the ASTER image of 2003 was complicated by large areas with low albedo at glacier tongues and middle moraines. A helpful tool in finding debris covered glacier parts in manual glacier mapping was the hue component of the IHS transformation in a FCC combination with ASTER band 2. The hue component displays also glacier parts in cast shadow and debris covered glacier ice. Unfortunately it was not possible to get any further information for some glaciers. This occurred in the case of some of the 14 disappeared glaciers for which still save relics may exist but covered with a debris or dirt layer. The mapped glacier area in 2003 is 36.89 km<sup>2</sup>.

Table 5.2 displays the number of glaciers in each class, the area of the classes and the percentage of the total area in 2003.

Class/km <sup>2</sup>	Number	Area/km <sup>2</sup>	Area/%
< 0.1	28	1.31	3.55
< 0.5	27	6.78	18.38
< 1.0	8	5.37	14.56
< 5.0	11	23.43	63.51
<b>Total</b>	74	36.89	100

Table 5.2: Statistics of the 2003 image for the 4 area classes. The area columns list the whole area and percentage of all glaciers in the area classes referring to the 2003 areas.

In class 1 (< 0.1 km<sup>2</sup>) the glacier SI 45 NN is the largest one with 0.05 km<sup>2</sup> and in class 2 (< 0.5 km<sup>2</sup>) it is Lisenser Ferner Berglas with 0.35 km<sup>2</sup>. In class 3 (< 1.0 km<sup>2</sup>) and 4 (< 5.0 km<sup>2</sup>) the largest glaciers are Berglas Ferner with 0.68 km<sup>2</sup> and Sulzenau Ferner with 4.09 km<sup>2</sup>. The total number of 74 glaciers in the ASTER images does not contain the 14 "disappeared" glaciers. The number of glaciers in each class refers, as mentioned before, to the glacier class classification of the ASTER images.

Figure 5.1 shows the division of the total area into the four classes a) in the Landsat, and b) in the ASTER image. The percentage inherited by each class refers in the Landsat image to the 116 glaciers. In the ASTER plot the percentage refers to the 74 glaciers, which are visible in the two images.

According to the number of glaciers in each class it is not surprising that the area class < 0.5 in the Landsat image is larger as the area class < 1.0. In the ASTER image the area class 1 covers 3.5% of area. Class 2 covers 19% of the total area. Figure 5.1 displays the large area changes in area class 2 and 3, whereas class 4 covers 62% of the total area.

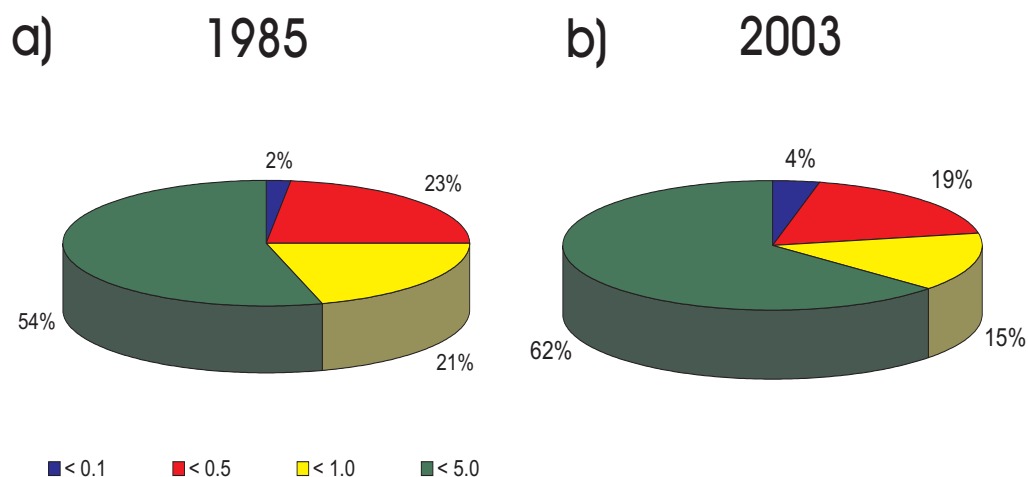


Figure 5.1: Area division a) for the Landsat 5 TM image of 30 September 1985 for the 117 glaciers. b) the ASTER image of 23 August 2003 for the 74 glaciers which are visible.

## 5.2.2 Area Changes 1985 - 2003

To quantify the changes in area between 1985 and 2003, the 88 glaciers of the ASTER image have been used for the calculation. The area of the 88 glaciers in the Landsat image is 54.42 km<sup>2</sup>. Table 5.3 shows the area of each class referring to 1985 and the total area in both images, the change in area in km<sup>2</sup> and the change in %.

Class/km <sup>2</sup>	Count	Area/km <sup>2</sup>		Change	
		1985	2003	km <sup>2</sup>	%
< 0.1	14	0.78	0.1	-0.68	-87.18
< 0.5	44	10.04	4.22	-5.82	-57.97
< 1.0	17	11.98	7.42	-4.56	-38.05
< 5.0	13	31.62	25.15	-6.47	-20.47
<b>Total</b>	88	54.42	36.89	-17.53	-32.21

Table 5.3: Summary data for the glacier area change between the Landsat image of 1985 and the ASTER image of 2003. The classes and the percentage refer to the 1985 glacier areas.

The accordance of increasing mean summer temperature towards the end of the period 1986 - 2003 and glacier retreat starting after 1985 is obvious from figure 5.2. In this figure the mean summer temperatures of Obergurgl located in Ötztal



are shown. A clear trend of increasing summer temperatures since the late 1980s is evident. "Large glaciers show a delay in dynamics to climate changes" from Kuhn, 2004 (Kuhn, 2004).

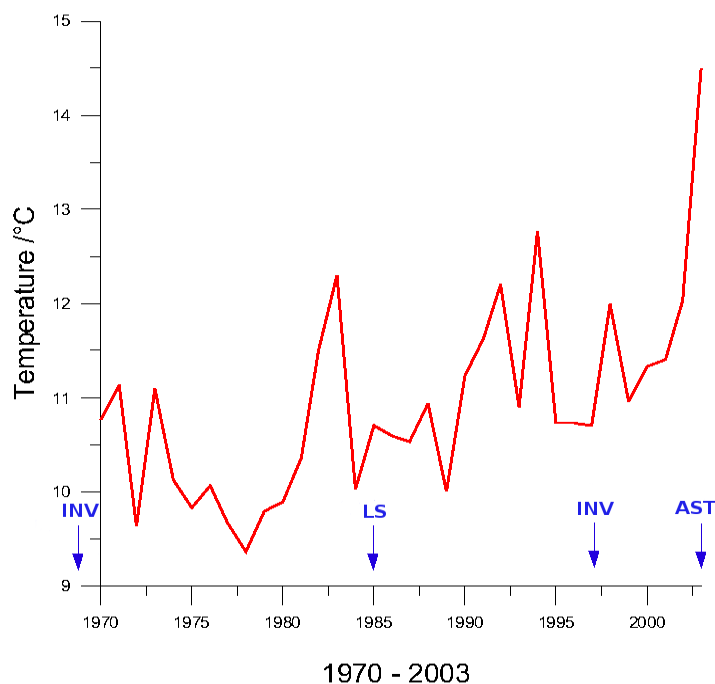


Figure 5.2: Mean summer temperatures of Obergurgl for the period 1970 - 2003.

Figure 5.3 illustrates the data of table 5.3. Figure 5.3a shows a part of southern Stubaital area with Sulzenau Ferner in the lower right of the image, and the two Scheiblehnferner glaciers in the upper part of the ASTER image. The red outlines are the glacier boundaries of the Landsat 5 TM image of 30 September 1985. The boundaries in magenta are of 23 August 2003. The small glaciers in the upper left cover half the area of 1985. The larger glaciers such as Sulzenau Ferner lost mass mainly in the terminal area and of glacier margins. Sulzenau Ferner has split into two parts, the Sulzenau Ferner part and the Fernerstube part. This example of Sulzenau Ferner also provides a hint on the volume change of glaciers. At the tongue of Sulzenau Ferner in 2003 two rock outcrops, one large and one small, were mapped, whereas in the 1985 boundaries and in the Landsat image no rock was visible in this part of the glacier. Figure 5.3b shows the relative area changes in percent between 1985 and 2003 for the 4 classes of 1985 and the total area. The area change in class 1 amounts to nearly 90% according to the 1985 classification of glaciers. Also in class 2 the loss in area amounts to more than 50%. Class 3 and class 4 show less reaction in area change. In total the loss in area is 32%. Figure

5.3b also shows the significant retreat in glacier area between 1985 and 2003.

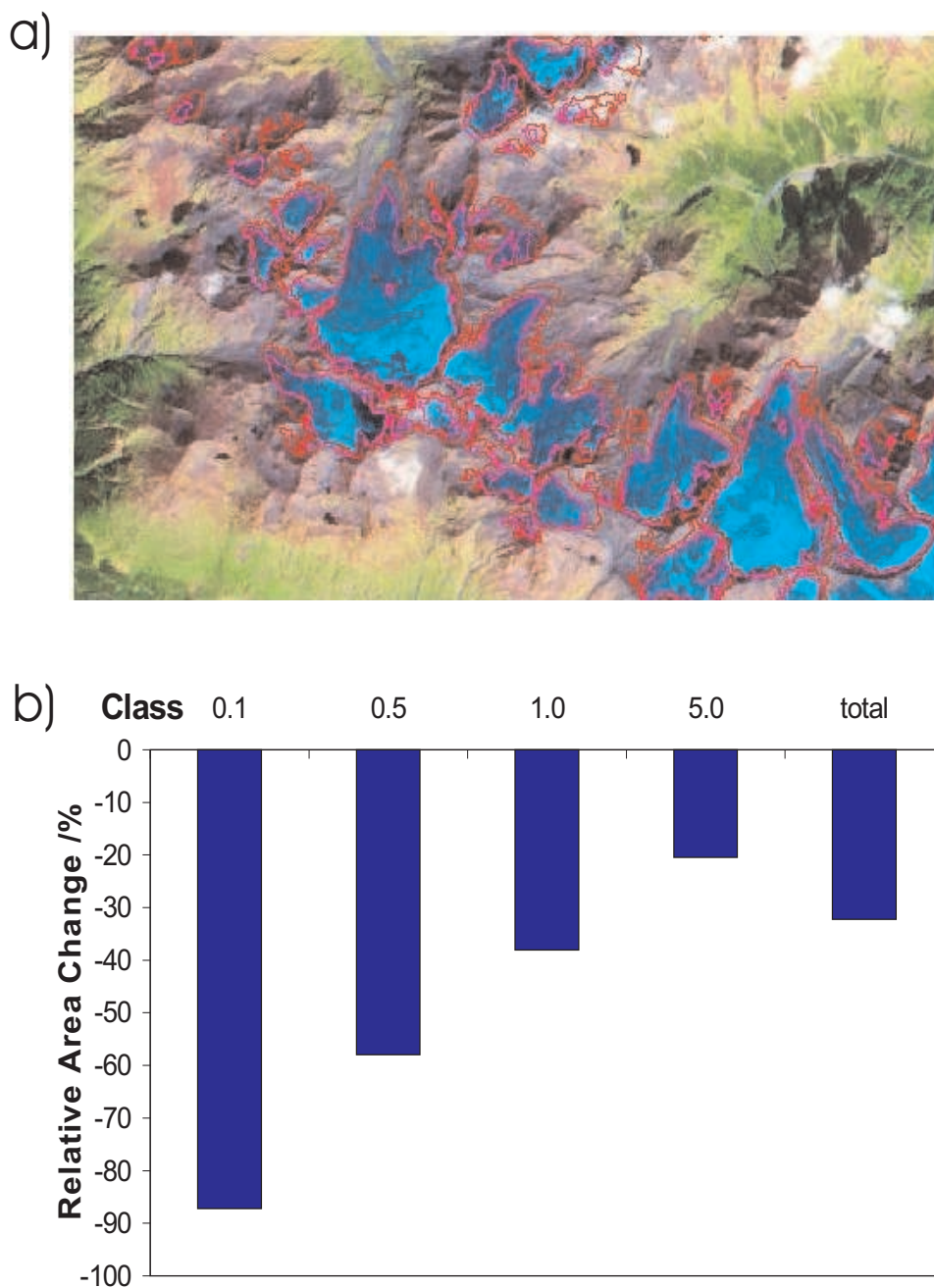


Figure 5.3: Relative area change displayed as a) glacier boundaries using an ASTER432 FCC image as background. Red are the boundaries of the Landsat image 1985 and magenta are the glacier boundaries of 2003. b) shows the relative area change for the 4 area classes of 1985 and the total area between 1985 and 2003.

Figure 5.4a shows the absolute area changes and figure 5.4b the relative area changes between 1985 and 2003 for each of the 88 glaciers in the ASTER image. The glacier size in the x-axis refers to 1985. Glaciers in class 4 increased their contribution to the entire glacier area by 10% whereas glaciers in class 1 and class 2 contribute 18.4% to the loss of the entire area.

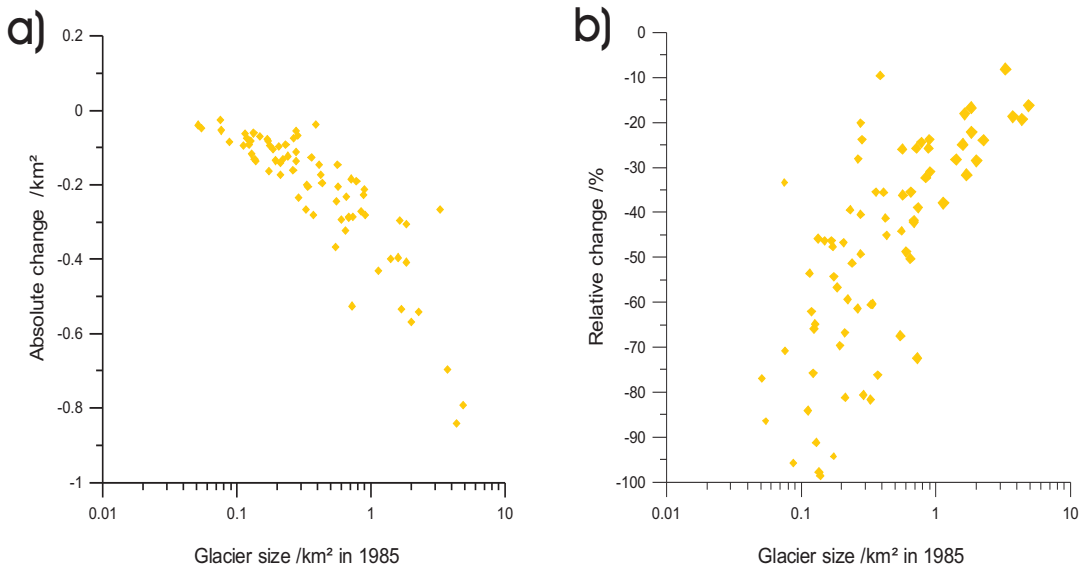


Figure 5.4: a) absolute area change between 1985 and 2003 and b) relative area change vs. glacier area in 1985 for the 88 glaciers.

Area change according to the exposition of the glaciers shows significant retreat in all expositions. The expositions of glaciers used here are expositions of the ablation zones. Table 5.4 shows the area loss according to the exposition. 5 glaciers with exposition SE lost 48% of their area although they cover only 2.5% of the total glaciated area. Only a single glacier has the exposition S and this lost also 48% of its area but covers only 0.8% of the total area. Statistic consideration is not possible as there is only one glacier in this class. Glaciers with ablation zone exposition N, NE and SW did not lose as much in percent as in the other expositions, but glaciers in N and NE are more frequent than in the other directions. In addition glaciers in SW exposition are not significant, as there are only two glaciers in that class.

In the period 1985 to 2003 not a single glacier increased in size. The values for each of the 88 glaciers is listed in tables B.4 to B.6 in appendix B. In the column with glacier names the suffix "Ferner" is not included because to save space.

Exposition	Count	Area/km <sup>2</sup>		Change	
		1985	2003	km <sup>2</sup>	%
N	29	22.7	15.54	-7.16	-31.5
NE	23	15.34	10.85	-4.49	-29.3
E	8	2.33	1.47	-0.86	-36.9
SE	5	1.79	0.93	-0.86	-48.0
S	1	0.6	0.31	-0.29	-48.3
SW	2	1.86	1.43	-0.43	-23.1
W	7	4.8	3.23	-1.57	-32.7
NW	13	5	3.1	-1.9	-38

Table 5.4: Area change between 1985 and 2003 according to the exposition in the ablation zone. Percentage refers to 1985.

## 5.3 Comparison with the Austrian Glacier Inventories

The satellite analysis was compared with the Austrian Glacier Inventories of 1969 and 1997 to obtain detailed information of glacier retreat during the last decades. Two different data sets for comparison were made. One is for the 117 glaciers between 1969 - 1985 - 1997 and the other is for the 88 glaciers in the ASTER image for the period 1969 - 1985 - 1997 - 2003. One of the goals is to show the glacier retreat beginning at the end of the 1980s and the accelerated retreat beginning in the mid 1990s.

The total glacier area in the airborne derived glacier inventory of 1969 was 63.06 km<sup>2</sup> (see chapter 3.3). In the Austrian Glacier Inventory of 1997 the glacier area amounts to 53.99 km<sup>2</sup>.

### 5.3.1 Comparison of the Landsat Data with the Austrian Glacier Inventories

The first comparison of glacier change is made between 1969 and 1985. The total area change in this period is less than 1 km<sup>2</sup> and amounts to 0.76 km<sup>2</sup>. Table 5.5 shows the area change for each class. Glacier OE 16 NN is included in this table, but because of its small size in 1969 it does not distort the result. Class 1 lost 0.085 km<sup>2</sup> in size which is very similar to the size of glacier OE 16 NN, which had 0.087

km<sup>2</sup> in 1969. Even in class 1 and 2 the area decreased only by a few percent. In total the change between 1969 and 1985 is very small. Several glaciers gained in size e.g. Sulzthal Ferner, which covered an area of 4.16 km<sup>2</sup> in 1969 and of 4.35 km<sup>2</sup> in 1985.

Class/km <sup>2</sup>	Count	Area/km <sup>2</sup>		Change	
		1969	1985	km <sup>2</sup>	%
< 0.1	18	1.26	1.18	-0.08	-6.7
< 0.5	66	15.23	14.33	-0.89	-5.9
< 1.0	18	12.85	23.89	0.35	0.4
< 5.0	15	33.72	33.88	0.16	0.5
<b>Total</b>	117	63.06	62.29	-0.76	-1.2

Table 5.5: Summary data for the glacier area change between the Austrian Glacier Inventory of 1969 and the Landsat image of 1985. Percentages refers to the 1969 area.

Some minor errors in the satellite data analysis are possible due to pixel size of the Landsat 5 TM sensor of 30m which may cause misclassification and misinterpretation of mixed pixels. During this period summer temperature did not show a clear trend (see figure 5.2).

Pronounced retreat in glacier area started after 1985. Between 1985 and 1997 glaciers in Stubaital lost 13.3% in area. Table 5.6 shows the area loss in the 4 classes. As expected relative losses in area were largest in class 2 and class 3. Although class 2 has 62 members it covers only 22% of the 1985 glacier area. Class 4 lost 8.9% in area in this period, it lost 3 km<sup>2</sup> between 1985 and 1997.

In figure 5.5 the absolute and relative changes in area between 1985 and 1997 are plotted. Some glaciers seem to have accumulated mass in this period according to figures 5.6a and 5.6b. It is possible that this is an apparent growth caused by underestimation of areas lying in cast shadow in the Landsat 5 TM image.

Class/km <sup>2</sup>	Count	Area/km <sup>2</sup>		Change	
		1985	1997	km <sup>2</sup>	%
< 0.1	19	1.2	1.08	-0.13	-10.45
< 0.5	63	13.81	10.74	-3.07	-22.23
< 1.0	20	14.42	10.4	-4.02	-27.91
< 5.0	14	32.91	29.97	-2.941	-8.94
<b>Total</b>	116	62.3	52.18	-10.16	-16.3

Table 5.6: Summary data for the glacier area change between the Landsat image of 1985 and the Austrian Glacier Inventory of 1997. Percentage refers to the 1985 area.

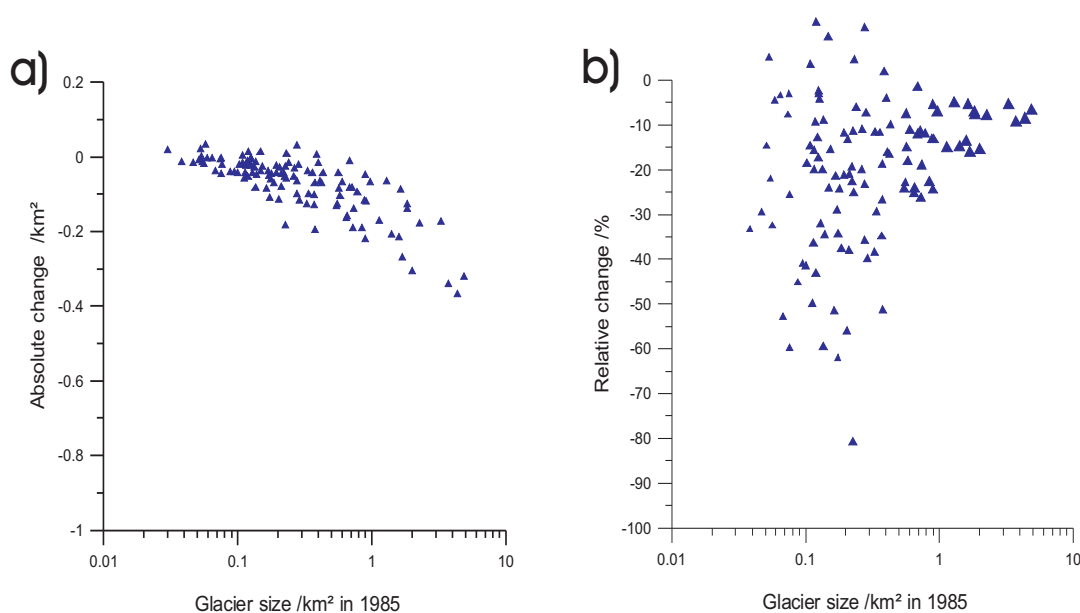


Figure 5.5: a) absolute area change between 1985 and 1997 and b) relative area change vs. glacier area in 1985 for the 116 glaciers.

### 5.3.2 Comparison of the ASTER Data with the Austrian Glacier Inventories

The comparison with the ASTER data was made again with the 88 mentioned glaciers. First, the results for the comparison with the Austrian Glacier Inventory of 1969 are discussed. As mentioned before, the change in glacier area was not significant in the period 1969 - 1985. So the change between 1969 and 2003 does not differ much from the change between 1985 and 2003. Again the relative loss in class 1 and class 2 is very high. The total loss in area between 1969 and 2003 amounts to 17.21 km<sup>2</sup> which corresponds to 31.8% of the 1969 area. Table 5.7 summarises the

area change for the period 1969 - 2003.

Class/km <sup>2</sup>	Count	Area/km <sup>2</sup>		Change	
		1969	2003	km <sup>2</sup>	%
< 0.1	13	0.95	0.11	-0.84	-88.9
< 0.5	46	10.73	4.51	-6.23	-58.0
< 1.0	14	11.24	7.10	-4.14	-36.8
< 5.0	13	31.15	25.14	-6.01	-19.3
<b>Total</b>	88	54.07	36.89	-17.21	-31.8

Table 5.7: Summary data for the glacier area change between the the Austrian Glacier Inventory of 1969 and the ASTER image of 2003. Percentages and count refer to the 1969 area.

Paul (Paul, 1995) used Landsat data and Landsat MSS data for a comparison between 1973 and 1992 of several glaciers located in western Austria and Switzerland. In Stubaital he mapped data of 57 glaciers, some located in Italy. He did not count small glaciers in his thesis because of the large pixel sizes in Landsat MSS data. He found out that the area change between 1985 and 1992 for large glaciers in Stubaital north was minus 10.2% and in Stubaital south minus 14.6%. In case of Sulzenau Ferner the loss in glacier area was 10% between 1985 and 1992. Ruderhof Ferner, located in northern Stubaital, lost 40.8% in this period. According to Paul's classification, class < 1km<sup>2</sup> lost 10.7% and class < 5km<sup>2</sup> lost 8.8% in northern Stubaital. Southern Stubaital lost 24.8% in class < 1km<sup>2</sup> and 11.9% in class < 5km<sup>2</sup>. In total Stubai glaciers lost 12.5% in area between 1985 and 1992. Paul's results is in qualitative agreement with the analysis of this thesis, but there are differences in details because of different methods and data sources for glacier mapping.

The comparison of the Austrian Glacier Inventory of 1997 with the ASTER data shows that the glaciers of Stubaital retreated much faster during this period than in earlier periods. Table 5.8 shows the area change in each class. Although the total relative change is less than in the periods 1969-2003 and 1985-2003, the time intervall is much shorter. The loss in area in class 1 between 1985 and 1997 is 30.2% referring to 1985 for the 88 glaciers. Between 1997 and 2003 the loss is 84.31% referring to 1997. So in class 1, 56% of area loss between 1985 and 2003 occurred during the years 1997 to 2003 referring to the 1985 glacier area. In total 75% of the 17.6km<sup>2</sup> loss in area in the period 1985 - 2003 was lost between 1997 and 2003.

Class/km <sup>2</sup>	Count	Area/km <sup>2</sup>		Change	
		1997	2003	km <sup>2</sup>	%
< 0.1	25	1.53	0.24	-1.29	-84.31
< 0.5	38	9.12	5.66	-3.46	-37.94
< 1.0	13	8.81	6.54	-2.27	-25.81
< 5.0	12	27.78	24.45	-3.33	-11.98
<b>Total</b>	88	47.24	36.86	-10.35	-21.9

Table 5.8: Summary data for the glacier area change between the the Austrian Glacier Inventory of 1997 and the ASTER image of 2003. Percentages refer to the 1997 area.

Figure 5.6a shows the absolute area change for the periods 1969 - 1985 (green), 1985 - 1997 (orange) and 1997 - 2003 (red). Figure 5.6b show the relative change for the three periods. Area changes for the period 1969 - 1985 refer to the glacier areas of 1969. Changes in the period 1985 - 1997 refer to the glacier areas of 1985 and changes in the period 1997 - 2003 refer to the areas of 1997.

The changes in the period 1969 - 1985 are small in relation to the changes in the other two periods. Relative area change in the period 1997 - 2003 is high for small glaciers and only five glaciers lost less than 10% in area. In both plots area changes in the period 1985 - 1997 are not higher than 60% except for two glaciers.

In tables B.7 to B.9 the area for all glaciers for the years 1969, 1985, 1997 and 2003 is shown. The changes are displayed in the three tables.



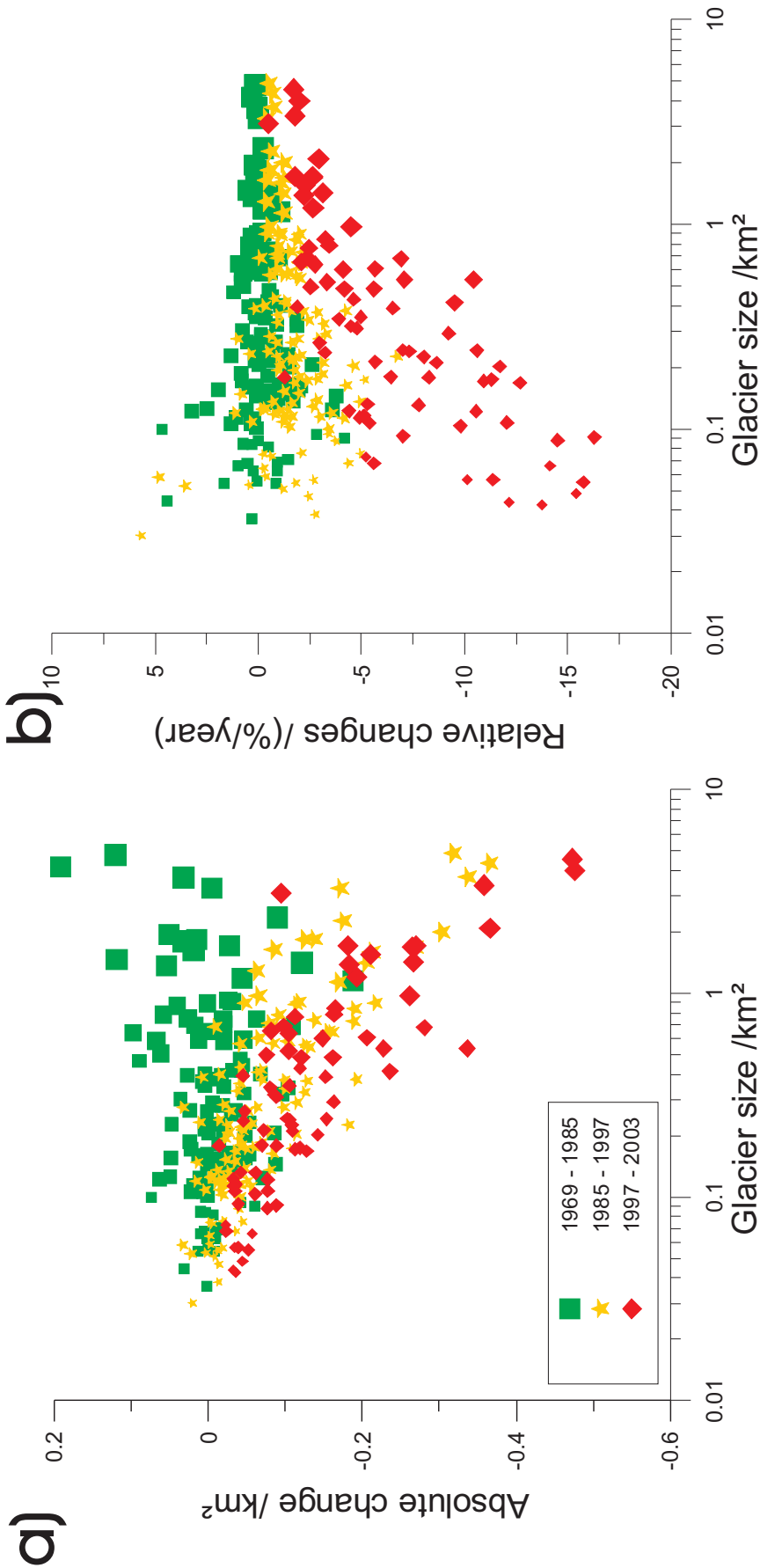


Figure 5.6: a) absolute area change of the four periods. b) relative area change vs. glacier area of the four periods. Changes in 1969 - 1985 refer to the glacier areas of 1969, in 1985 - 1997 they refer to the glacier areas of 1985 and in the period 1997 - 2003 the changes refer to the areas of 1997.

## 5.4 Snow Coverage on Glaciers in 1985

As mentioned before all glaciers except one were visible in the Landsat image of 1985. The snow cover maps derived from the NDSI (see section 4.1.4) were converted into snow cover boundaries and their area has been calculated. Not all glaciers had winter snow left, and many glaciers smaller than  $1.0 \text{ km}^2$  belong to this group without winter snow cover. Of the 17 glaciers  $< 0.1 \text{ km}^2$  only 8 had snow covered areas. In class 2,  $< 0.5 \text{ km}^2$ , 41 of 66 had snow cover. Snow covers 15.6% of the total glacier area in this class. For glaciers larger than  $0.5 \text{ km}^2$  only one glacier, Simming Ferner M, had no winter snow cover left. The total glacier area of the 1985 image was  $62.28 \text{ km}^2$ , and the snow on the glaciers covered  $19.61 \text{ km}^2$ . This shows that 31% of the glacier area in late summer 1985 were snow covered, pointing out that overall the mass balance was clearly negative. In Austria the accumulation area ratio for glaciers the ratio of  $S_c/S$ .  $S_c$  is the accumulation area,  $S$  is the total glacier area.  $S_c/S$  is  $\approx 0.7$  for balanced budget for Austrian glaciers.

What becomes apparent in case of Simming Ferner M is that NDSI works poorly in cast shadow areas. Simming Ferner M is one of 13 glaciers in the south western range of the Stubai glaciers, which are located in an area with cast shadow in the Landsat 5 TM image. For all those glaciers errors in NDSI area size are possible.

Table 5.9 summarises the results of the snow classification.

Class/ $\text{km}^2$	Count		Area/ $\text{km}^2$		%
	1985	Snow	1985	Snow	
$< 0.1$	17	8	1.18	0.12	9.9
$< 0.5$	66	41	14.3	2.23	15.6
$< 1.0$	18	17	12.89	3.72	28.8
$< 5.0$	15	15	33.87	13.54	40
<b>Total</b>	117	81	62.28	19.61	31

Table 5.9: Summary data for the snow/firn covered glacier area of 1985.

Best results show class 4 with 40% snow covered glacier area. In the ASTER image of 2003 there is not much snow left on the glaciers, in these areas were probably firn from previous years (névé).

# Chapter 6

## Summary and Conclusion

The main objective of the thesis was to map the extend and recent changes of Stubai glaciers using satellite images. The database included Landsat and ASTER images. Comparisons were made with data of the Austrian Glacier Inventories. The work is also a contribution to the GLIMS initiative "Global Land Ice Measurements from Space" of USGS.

One Landsat 5 TM image of 30 September 1985 and two ASTER images of 23 August 2003 were available for the analysis. Glacier sizes of the Austrian Glacier Inventories were provided from Astrid Lambrecht. The Landsat 5 TM of the study region is cloud free whereas in both ASTER images several glaciers are covered partly or totally by clouds or cloud shadows.

After orthorectification of the satellite images glacier boundaries were mapped manually in all three satellite images. In total 190 boundaries were made. In the Landsat image 116 glaciers were mapped, in the ASTER images in total 74 glaciers were mapped. Manual glacier mapping is time consuming in mapping and in compiling attribute tables. The attribute tables contain the WGMS glacier code, glacier name, glacier size, shape length, glacier class in the image, former glacier class and exposition in accumulation and ablation area. Also glacier ID points, which contain longitude and latitude of glaciers, were added to the attribute tables. In debris covered areas and cast shadow the glacier boundaries could not be clearly identified on some glaciers.

For the ASTER image difficulties with debris cover with automatic classification arose therefore only manually derived glaciers sizes were used. Bitmaps of glacier areas were produced from ratio images of NIR/SWIR channels on surfaces with clean snow and glacier ice outside of shadow areas.

The NDSI (Normalised Difference Snow Index) was used to map snow covered areas. For both satellites snow cover masks were made. Whereas in the Landsat image

substantial snow cover on glaciers was observed, the ASTER image except for some of the larger glaciers ( $< 5.0 \text{ km}^2$ ) barely shows snow covered areas. Here the IHS (Intensity - Hue - Saturation) transformation was used for a comparison with the ratio derived snow mask. The saturation component of the transformation proved to be an alternative to the NDSI.

The unsupervised and supervised classifications were made according to GLIMS Algorithm Working Group (Kääb, 2004) to investigate possible differences for glacier mapping of the various methods, but was not used further for obtaining any other information in this thesis.

For mapping debris cover on glaciers two approaches were used. One approach was an algorithm using NIR and SWIR channels which turned out to be accurate on glaciers but also classified rocky areas. The other approach used was again the IHS transformation. The hue component showed debris covered glacier areas and also ice and snow in cast shadow. With the information derived from the hue component about ice and snow in cast shadow and debris cover some debris covered glacier tongues were remapped. Also some glaciers in cast shadow were reanalysed.

As additional tools to the GLIMS Algorithm Working Group Paul, 2003 (Paul, 2003) recommends using the IHS transformation and the PCA (principal component analysis). The IHS transformation turned out to be helpful for analysing debris covered and cast shadow areas. Also for analysing snow cover on glaciers it is an alternative to the NDSI as well as PCA. PC3 of the ASTER image and PC4 of the Landsat image can be used to map snow cover on glaciers.

The resulting glacier areas of the Landsat image show little differences compared to the Austrian Glacier Inventory of 1969. Some glaciers even increased in size. Some problems occurred with glaciers which were partly in cast shadow. One glacier could not be mapped at all due to cast shadow. Total area loss between 1969 and 1985 amounts to 1.2%.

The comparison with the Austrian Glacier Inventory of 1997 revealed significant glacier retreat that started after 1985. Area class  $< 0.1 \text{ km}^2$ , which contains 18 members, and area class  $< 0.5 \text{ km}^2$ , which contains 88 members, lost between 20 - 25% in area. Small glaciers showed larger relative changes than larger glaciers.

The ASTER derived glacier boundaries of 2003 revealed also significant glacier retreat, starting after 1985 and accelerating between 1997 and 2003. This acceleration in glacier retreat is in accordance with a clear trend of increasing summer temperatures starting in the mid 1980s and amplifying towards the end of the period 1969 - 2003. Area changes in periods 1969 - 1985 showed no large changes in glacier areas. Between 1985 - 1997 glaciers in Stubaital lost 13%. The retreat between 1997 and

2003 is 22% what supports the assumption of increasing retreat after 1985.

In analysing the results of this study the massive glacier retreat between 1997 and 2003 was surprising. A retreat in glacier area was expected but not by such dimensions in this short period of time. A main reason for the strong retreat of glaciers in the study region is the small average size of the glaciers, especially small glaciers are sensitive to climate changes.



# Bibliography

- Berthier, E., Y. Arnaud, D. Baratoux, C. Vincent and F. Rémy (2004). Recent rapid thinning of the "Mer de Glace" glacier derived from satellite optical images, *Geophysical Research Letters*.
- Chander, G. and B. Markham (2003). Revised Landsat-5 TM Radiometric Calibration Procedures and Postcalibration Dynamic Ranges, *IEEE Transactions on Geoscience and Remote Sensing*.
- Copeland, L. (1995). *GLIMS Databasing Guide for the University of Alberta Regional Center*, University of Alberta.
- Eder, K., R. Würlländer and H. Rentsch (2000). Digital Photogrammetry for the new Glacier Inventory of Austria, Vol. XXXIII, IAPRS, Amsterdam.
- Epema, G. (1990). Determination of Planetary Reflectance for the Landsat-5 Thematic-Mapper Tapes Processed by Earthnet (Italy), *ESA Journal*.
- GLIMS (1995). GLIMS - Global Land Ice Measurements from Space, <http://www.glims.org/>.
- Greuell, W. and M. de Ruyter de Wildt (1999). Anisotropic Reflection by Melting Glacier Ice: Measurements and Parametrizations in Landsat TM Bands 2 and 4, *Remote Sensing of Environment* **70**, 265 – 277.
- Groß, G. (1987). Die Flächenänderung der Österreichischen Gletscher, *Zeitschrift für Gletscherkunde und Glazialgeologie* **23**(2), 131–141.
- Hall, D., A. Chang, J. Foster, C. Benson and W. Kovalick (1989). Comparison of in situ and Landsat derived reflectances of Alaskan glaciers, *Remote Sensing of Environment* **28**, 493 – 504.
- Hall, D., K. Bayr, W. Schöner, R. Bindschadler and J.Y.L.Chien (2003). Consideration of the errors inherent in mapping historical glacier positions in Austria

- from the ground and space (1893 - 2003), *Remote Sensing of Environment* **86**, 566 – 577.
- JPL (2005). ASTER spectral library, <http://speclib.jpl.nasa.gov>.
- Kääb, A. (2004). *GLIMS algorithm document*, GLIMS.
- Knap, W. and C. Reijmer (1998). Anisotropy of the Reflected Radiation Field Over Melting Glacier Ice: Measurements in Landsat TM Bands 2 and 4, *Remote Sensing of Environment* **65**, 93 – 104.
- Kuhn, M. (2004). Klima und Kryosphäre, Lecture.
- Nagler, T. (1996). *Methods and Analysis of Synthetic Aperture Radar Data from ERS-1 and X-Sar for Snow and Glacier Applications*, PhD thesis, University Innsbruck.
- NSIDC (visited 2005). National Snow and Ice Data Center, <http://www.nsidc.org>.
- Paterson, W. S. B. (1994). *The physics of glaciers*, Butterworth Heinemann.
- Paul, F. (1995). *Fernerkundung von Gletscheränderungen in den Alpen zwischen 1973 and 1992 mit Landsat*, Master's thesis, Universität Hamburg.
- Paul, F. (2002D). Changes in glacier area in Tyrol, Austria, between 1969 and 1992 derived from Landsat 5 TM and Austrian glacier inventory data, *International Journal of Remote Sensing* **23**(4), 787–799.
- Paul, F. (2003). *The New Swiss Glacier Inventory 2000*, PhD thesis, ETH Zurich.
- Peipe, J., P. Reiss and H. Rentsch (1978). Zur Anwendung des Digitalen Geländemodells in der Gletscherforschung, *Zeitschrift für Gletscherkunde und Glazialgeologie* **14**(2), 161–172.
- Rau, F., F. Mauz, S. Khalsa and B. Raup (2005). *Illustrated GLIMS Glacier Classification Manual*, Institut für Physische Geographie Freiburg, NSIDC.
- Raup, B. (1996). *Processing plan for GLIMS*, NSIDC.
- Raup, B. and S. Khalsa (2005). *GLIMS Analysis Tutorial*, NSIDC.
- Rentsch, H., W. Welsch, C. Heipke and M. Miller (1990). Digital Terrain Models as a Tool for Glacier Studies, *Journal of Glaciology* **36**(124), 273–278.



- Richards, J. (2005). *Remote Sensing Digital Image Analysis*, 2nd edition, Springer Verlag, Berlin Heidelberg.
- Rott, H. (1976). Analyse der Schneeflächen auf Gletschern der Tiroler Zentralalpen aus Landsat Bildern, *Zeitschrift für Gletscherkunde und Glazialgeologie* **12**, 1–28.
- Rott, H. and G. Markl (1989). Improved Snow and Glacier Monitoring by the Landsat Thematic Mapper, in Guyenne, T. and G. Calabresi (ed.), *Monitoring the Earth's Environment*, Vol. SP-1102, pp. 3–12.
- Schwikowski, M., B. Rufibach, A. Schwerzmann, D. Stampfli, C. Barbante, F. Planchon, P. Gabrielli and C. Boutron (2005). Two new ice cores from Colle Gnifetti, Swiss/Italian Alps, <http://lch.web.psi.ch/pdf/anrep03/28.pdf/>.
- Sidjak, R. W. and R. Wheate (1999). Glacier mapping of the illecillewaet icefield, british columbia, canada, using landsat tm and digital elevation data, *International Journal of Remote Sensing* **20**(2), 273–284.
- Smith, A. (2005). How to Convert ASTER Radiance Values to Reflectance, <http://www.cnrhome.uidaho.edu/>.
- USGS-EROS (visited October 2005). Landsat Thematic Mapper Data, [http://eros.usgs.gov/guides/landsat\\_tm.html](http://eros.usgs.gov/guides/landsat_tm.html).
- Wechselberger, F. and L. Wechselberger (visited 2006). Berge-Tirol.at, <http://www.berge-tirol.at>.
- Wiscombe, W. J. and S. Warren (1980). A model for the spectral reflectance of snow. I: Pure snow, *Journal of the Atmospheric Sciences* **37**, 2712 – 2733.



# Appendix A

## Software

In this thesis a variety of software was used. For processing the Landsat 5 TM and the ASTER data the commercial software PCI Geomatics was used. Used modules of PCI are *XPACE* for interactive data processing, *GCPWORKS* for the collection of Ground Control Points (GCP's), *imageworks* for classification and data visualisation and *EASI Modelling Tool* for direct data modelling in *imageworks*. ArcView is used for creating the glacier ID-points, the central flowlines and the resulting glacier shapefiles and tables which are send to the GLIMS-database. For data evaluation of the glaciers sizes and comparison with the Austrian Glacier Inventory of 1969 and 1997 Microsoft's office tool Excel was used.

The graphics have been made using *The GIMP*, an image editor, and *Corel Draw Essentials 2 SE*. Frequently applied software was *ghostscript* for the conversion ps to jpg, ps to eps.



# Appendix B

## Tables

Size	Class
$< 0.1 \text{ km}^2$	1
$0.1 \text{ to } < 0.5 \text{ km}^2$	2
$0.5 \text{ to } < 1.0 \text{ km}^2$	3
$1.0 \text{ to } < 5.0 \text{ km}^2$	4

Table B.1: Glacier classes in Stubaital area.

River	Number	Glacier	Class 1969
ME	7	Winnebach Ferner E	1
ME	13	Griesskogel Ferner E	1
OE	1	Gamezkogel Ferner	2
OE	3	Mittertal Ferner	2
OE	10	Winnebach Ferner M	1
OE	16	NN	1
OE	25	NN	1
OE	26	NN	1
OE	27	Wannen Ferner	2
OE	30	Muschen Ferner E	2
OE	49	Schrakar Ferner	2
OE	51	Rötenkar Ferner	2
SI	50	Knotenspitz Ferner M	2
SI	51	Knotenspitz Ferner W	1

Table B.2: Glaciers, which no longer exist or are completely debris covered in the ASTER image on the 23<sup>rd</sup> August 2003

River	Number	Glacier	Class 1969
ME	1	Fotscher Ferner	2
OE	44	Östlicher Scheiblehn Ferner W	2
OE	45	Westlicher Scheiblehn Ferner	2
OE	46	Hangender Ferner	2
OE	47	Kitzkampf Ferner	2
SI	10	NN	2
SI	11	Padreil Ferner	2
SI	12	Simming Ferner E	2
SI	13	Simming Ferner M	3
SI	14	Simming Ferner W	3
SI	15	Aperer Feuerstein Ferner E1	1
SI	16	Glätte Ferner	2
SI	17	Habicht Ferner	1
SI	18	Pinnis Ferner	1
SI	19	Äusserer Mischbach Ferner	2
SI	20	Aperer Feuerstein Ferner E2	2
SI	21	Aperer Feuerstein Ferner W	2
SI	22	NN	2
SI	23	Östlicher Grübl Ferner	4
SI	24	Östlicher Grübl Ferner oben	2
SI	25	Westlicher Grübl Ferner E	2
SI	26	Westlicher Grübl Ferner M	2
SI	29	Kleiner Grünau Ferner	2
SI	40	Ruderhof Ferner unten	2
SI	41	Ruderhof Ferner oben	1
SI	42	Grawawand Ferner	2
SI	43	Hochmoos Ferner	4
SI	47	Jedlasgrübl Ferner	1
SI	48	Gugeliger Ferner	2

Table B.3: Glaciers, which are not visible in the ASTER image on the 23<sup>rd</sup> August 2003 due to clouds or shadow

WGS-Code		Name	Area/km <sup>2</sup>		Change/%	Class'69	Exp.	
FL	No		1985	2003				
ME	2	Lisenser	3.28	3.01	-8.1	4	NE	
ME	3	Rotgrat	0.26	0.19	-28.1	2	NE	
ME	4	Längentaler	0.68	0.39	-42.2	3	N	
ME	5	Grüne Tatzten	0.18	0.08	-54.3	2	SE	
ME	6	Ochsenkar	0.33	0.06	-81.7	2	NE	
ME	7	Winnebach E	0.05			1	NE	
ME	8	Weißkogel	0.18	0.08	-56.7	2	SE	
ME	9	Zischgeles	0.28	0.14	-49.2	2	N	
ME	10	Gleirsch	0.84	0.57	-32.3	3	N	
ME	11	S. Sonnenwand	0.21	0.07	-66.8	2	NE	
ME	12	N. Sonnenwand	0.17	0.09	-47.6	2	NE	
ME	13	Griesskogel E	0.08			1	N	
ME	14	Griesskogel W	0.14	0.002	-98.6	2	N	
ME	15	Kraspes	0.73	0.20	-72.4	3	N	
OE	1	Gamezkogel	0.15			2	N	
OE	2	Längentaler	0.17	0.01	-94.3	1	N	
OE	3	Mittertal	0.20			2	N	
OE	4	Steinkar	0.14	0.003	-97.8	2	E	
OE	5	Zwiselbach	0.64	0.32	-50.2	3	N	
OE	6	Zwiselbach W	0.15	0.08	-46.3	2	NE	
OE	7	Larstig	0.65	0.42	-35.5	3	N	
OE	8	Grastal	0.78	0.59	-24.4	3	W	
OE	9	Griesskogel	0.56	0.31	-44.1	2	SE	
OE	10	Winnebach M	0.09			1	NW	
OE	11	Winnebach W	0.17	0.09	-46.3	2	NW	
OE	12	Bachfallen	2.26	1.72	-23.9	4	N	
OE	13	Putzenkar	0.12	0.03	-75.8	2	N	
OE	14	Säuischbach	0.28	0.22	-23.8	2	N	
OE	15	S. Schrankar	0.28	0.22	-20.2	2	NW	
OE	16	NN	too much shadow				1	NW
OE	17	Schwarzenberg	1.64	1.34	-18.0	4	SW	
OE	18	Bockkogel E	0.71	0.53	-25.8	3	NW	
OE	19	Bockkogel W	0.56	0.42	-28.9	3	NW	
OE	20	NN	0.21	0.11	-46.7	2	N	
OE	21	NN	0.05	0.01	-76.9	1	NW	
OE	22	Sulztal	4.35	3.51	-19.3	4	N	
OE	23	NN	0.13	0.07	-45.9	2	NE	
OE	24	Kuhscheiben	0.41	0.26	-35.6	2	NE	

Table B.4: Part one of the comparison of the 88 glaciers, which are visible in the ASTER image, and their changes between 1985 and 2003. Percentages refer to 1985.

WGS-Code		Name	Area/km <sup>2</sup>		Change/%	Class'69	Exp.
FL	No		1985	2003			
OE	25	NN	0.04			1	NE
OE	26	NN	0.07			1	NE
OE	27	Wannen	0.11			2	N
OE	28	Rosskar	0.26	0.10	-61.4	2	N
OE	29	NN	0.12	0.04	-65.9	2	NE
OE	30	Muschen E	0.11			2	N
OE	31	Muschen W	0.21	0.04	-81.2	2	N
OE	32	Reichenkar	0.05	0.007	-86.5	1	NE
OE	33	Atterkar	0.36	0.23	-35.4	2	NW
OE	34	Wütenkar	1.41	1.01	-28.3	4	NW
OE	35	Wildkar	0.08	0.004	-95.8	1	NW
OE	36	Warenkar	0.60	0.30	-50.0	3	S
OE	37	Windacher	0.43	0.23	-50.0	2	W
OE	38	NN	0.13	0.04	-64.9	2	W
OE	39	Gaisskar	0.69	0.39	-43.4	3	SE
OE	40	Pfaffen	1.14	0.70	-37.9	4	W
OE	41	Triebenkarlas	1.83	1.52	-16.8	4	W
OE	42	Ö. Scheiblehn E ob.	0.22	0.09	-59.3	2	SW
OE	43	Ö. Scheiblehn E	0.33	0.13	-60.5	2	W
OE	48	Kitzkamp W	0.29	0.06	-80.6	2	N
OE	49	Schrakar	0.23			2	NE
OE	50	Haglkar	0.11	0.02	-84.1	2	NE
OE	51	Rötenkar	0.16			2	W
SI	27	W. Grübl W	0.74	0.45	-38.9	3	NE
SI	28	NN	0.08	0.02	-70.8	1	E
SI	30	Grünau	1.84	1.43	-22.1	4	N
SI	31	Aperer Freiger	0.37	0.09	-76.2	2	NW
SI	32	Sulzenau	4.88	4.09	-16.2	4	N
SI	33	NN	0.12	0.05	-62.1	2	N
SI	34	Fernau	1.99	1.42	-28.5	4	N
SI	35	Schaufel	1.69	1.15	-31.7	4	NE
SI	36	Daunkogel	1.59	1.19	-24.9	4	NE
SI	37	Daunkopf	0.54	0.18	-67.4	3	NE
SI	38	Großer See	0.19	0.06	-69.6	2	SE
SI	39	Hölltal	0.24	0.12	-50.0	2	E
SI	44	Falbesoner Kräul	0.23	0.14	-34.5	2	E
SI	45	NN	0.08	0.05	-33.4	1	E
SI	46	Falbesoner Knoten	0.42	0.24	-41.3	2	NE

Table B.5: Part two of the comparison of the 88 glaciers, which are visible in the ASTER image, and their changes between 1985 and 2003. Percentages refer to 1985.



WGS-Code		Name	Area/km <sup>2</sup>		Change/%	Class'69	Exp.
FL	No		1985	2003			
SI	49	Knotenspitz E	0.12	0.05	-53.5	2	N
SI	50	Knotenspitz M	0.06			2	N
SI	51	Knotenspitz W	0.03			1	N
SI	52	Sommerwand	0.88	0.65	-25.8	3	N
SI	53	Alpeiner Kräul	0.57	0.36	-36.2	3	NW
SI	54	Seespitz	0.34	0.13	-60.4	2	NW
SI	55	Alpeiner	3.73	3.03	-18.7	4	NE
SI	56	Verborgten Berg	0.91	0.62	-30.9	3	E
SI	57	Turm	0.28	0.16	-40.5	2	E
SI	58	Berglas	0.89	0.68	-23.8	3	NE
SI	59	Berglas N	0.13	0.01	-91.2	2	NE
SI	60	Lisenser Berglas	0.39	0.25	-9.6	2	E
<b>Total</b>		<b>88 glaciers</b>	<b>54.42</b>	<b>36.86</b>	<b>-32.3</b>		

Table B.6: Part three of the comparison of the 88 glaciers, which are visible in the ASTER image, and their changes between 1985 and 2003. Percentages refer to 1985.

WGS-Code FL	No	Name	Area /km <sup>2</sup>			Change /%				Class		
			'69	'85	'97	'03	'69-85	85-97	85-03		97-03	69-03
ME	1	Fotscher	0.16	0.11	0.11		-33.1	3.6				2
ME	2	Lisenser	3.28	3.28	3.1	3.01	-0.1	-5.2	-8.1	-3.1	-8.3	4
ME	3	Rotgrat	0.26	0.26	0.24	0.19	0.8	-10.9	-28.1	-19.3	-27.6	2
ME	4	Längentaler	0.75	0.69	0.68	0.39	-8.3	-1.3	-42.2	-41.5	-47.0	3
ME	5	Grüne Tatzen	0.13	0.16	0.12	0.08	39.5	-34.2	-54.3	-30.6	-36.5	2
ME	6	Ochsenkar	0.35	0.33	0.2	0.06	-5.7	-38.8	-81.7	70.3	-81.7	2
ME	7	Winnebach E	0.05	0.05	0.03		-13.9	-29.4				1
ME	8	Weisskogel	0.12	0.18	0.12	0.08	51.7	-37.5	-56.7	-30.8	-34.4	2
ME	9	Zischgeles	0.28	0.28	0.21	0.14	-2.2	-23.1	-49.2	-34.0	-50.3	2
ME	10	Gleirsch	0.78	0.84	0.65	0.57	7.5	-22.6	-32.3	-12.6	-27.2	3
ME	11	S. Sonnenwand	0.19	0.21	0.13	0.07	13.2	-37.8	-66.8	-46.6	-62.4	2
ME	12	N. Sonnenwand	0.16	0.17	0.12	0.09	7.8	-28.8	-47.6	-26.4	-43.5	2
ME	13	Griesskogel E	0.04	0.07	0.03		70.9	-59.6				1
ME	14	Griesskogel W	0.17	0.14	0.09	0.002	-16.2	-34.5	-98.6	-97.8	-98.8	2
ME	15	Kraspes	0.75	0.72	0.54	0.20	-2.6	-26.1	-72.4	-62.7	-73.2	3
OE	1	Gamezkogel	0.2	0.15	0.13		-23.9	-15.3				2
OE	2	Längentaler	0.1	0.17	0.07	0.01	75.0	-61.9	-94.3	-84.9	-89.9	1
OE	3	Mittertaler	0.16	0.20	0.09		30.9	-55.8				2
OE	4	Steinkar	0.12	0.14	0.05	0.003	9.2	-59.4	-97.8	-94.5	-97.6	2

Table B.7: Glacier area of all 117 glaciers for the years 1969, 1985, 1997, 2003 and the changes for the periods 1969 - 1985, 1985 - 1997, 1985 - 2003, 1997 - 2003 and 1969 - 2003.

WGS-Code	Name	Area/km <sup>2</sup>			Change/%				Class		
		'69	'85	'97	'03	69-85	85-97	85-03		97-03	69-03
OE 5	Zwieselbach	0.65	0.64	0.48	0.32	-0.5	-25.1	-50.2	-33.6	-50.5	3
OE 6	Zwieselbach W	0.15	0.15	0.11	0.08	-3.4	-23.9	-46.3	-29.5	-48.2	2
OE 7	Larstig	0.58	0.65	0.5	0.42	11.6	-23.9	-35.5	-15.2	-28.1	3
OE 8	Grastal	0.75	0.78	0.69	0.59	3.52	-11.8	-24.4	-14.2	-21.7	3
OE 9	Griesskogel	0.46	0.56	0.43	0.31	19.4	-22.7	-44.1	-27.7	-33.3	2
OE 10	Winnebach M	0.08	0.09	0.06		11.9	-40.8				1
OE 11	Winnebach W	0.18	0.17	0.13	0.09	-7.4	-21.3	-46.3	-31.8	-50.3	2
OE 12	Bachfallen	2.35	2.26	2.08	1.72	-3.8	-7.8	-23.9	-17.6	-23.9	4
OE 13	Putzenkar	0.14	0.12	0.11	0.03	-9.4	-12.7	-75.8	-72.3	-78.1	2
OE 14	Säuischbach	0.29	0.28	0.26	0.22	-1.9	-7.3	-23.8	-17.9	-25.3	2
OE 15	S. Schrankar	0.32	0.28	0.31	0.22	-14.2	-11.9	-20.2	-28.6	-31.58	2
OE 16	NN	0.09		0.05							1
OE 17	Schwarzenberg	1.62	1.64	1.55	1.34	1.2	-5.2	-18.1	-13.6	-17.1	4
OE 18	Bockkogel E	0.7	0.71	0.63	0.53	2.6	-11.2	-25.8	-16.4	-23.9	3
OE 19	Bockkogel W	0.58	0.56	0.52	0.42	-3.5	-7.4	-25.9	-20.0	-28.6	3
OE 20	NN	0.21	0.21	0.18	0.11	-0.4	-13.2	-46.7	-38.7	-46.9	2
OE 21	NN	0.09	0.05	0.04	0.012	-45.6	-14.6	-76.9	-73.1	-87.5	1
OE 22	Sulztal	4.16	4.35	3.99	3.51	4.6	-8.4	-19.4	-11.9	-15.6	4
OE 23	NN	0.11	0.13	0.11	0.07	16.9	-19.9	-45.9	-32.4	-36.7	2
OE 24	Kuhscheiben	0.4	0.41	0.34	0.26	1.2	-15.9	-35.6	-23.4	-34.8	2
OE 25	NN	0.04	0.04	0.03		5.01	-33.2				1

Table B.8: Glacier area of all 117 glaciers for the years 1969, 1985, 1997, 2003 and the changes for the periods 1969 - 1985, 1985 - 1997, 1985 - 2003, 1997 - 2003 and 1969 - 2003.

WGS-Code		Name	Area/km <sup>2</sup>			Change/%				Class		
FL	No		'69	'85	'97	'03	69-85	85-97	85-03		97-03	69-03
OE	26	NN	0.05	0.07	0.03		26.1	-52.7				1
OE	27	Wannen	0.16	0.11	0.09		-30.7	-14.5				2
OE	28	Rosskar	0.28	0.26	0.21	0.10	-6.6	-19.8	-61.4	-51.9	-63.9	2
OE	29	NN	0.15	0.12	0.1	0.04	-16.5	-17.2	-65.9	-58.8	-71.5	2
OE	30	Muschen E	0.15	0.11	0.07		-25.3	-36.3				2
OE	31	Muschen W	0.23	0.21	0.17	0.04	-7.1	-20.9	-81.2	-76.2	-82.5	2
OE	32	Reichenkar	0.07	0.05	0.04	0.007	-23.0	-21.9	-86.5	-82.7	-89.6	1
OE	33	Attenkar	0.35	0.36	0.32	0.23	1.44	-11.6	-35.4	-26.9	-34.5	2
OE	34	Wütenkar	1.36	1.41	1.21	1.01	3.9	-14.6	-28.3	-16.0	-25.4	4
OE	35	Wildkar	0.08	0.09	0.05	0.004	4.6	-45	-95.8	-92.4	-95.6	1
OE	36	Warenkar	0.59	0.60	0.54	0.31	2.2	-10.9	-48.4	-42.5	-47.7	3
OE	37	Windacher	0.47	0.43	0.39	0.24	-8.7	-9.8	-45.1	-39.2	-49.9	2
OE	38	NN	0.16	0.13	0.12	0.05	-20.4	-4.2	-64.9	-63.3	-72	2
OE	39	Gaisskar	0.71	0.68	0.6	0.39	-2.7	-11.8	-41.8	-34.0	-43.4	3
OE	40	Pfaffen	1.18	1.14	0.97	0.71	-3.7	-14.9	-37.9	-27.1	-40.2	4
OE	41	Triebenkarlas	1.79	1.83	1.7	1.52	1.8	-6.8	-16.8	-10.7	-15.3	4
OE	42	Ö. Scheiblehn E ob.	0.22	0.22	0.18	0.09	2.6	-19.3	-59.3	-49.6	-58.3	2
OE	43	Ö. Scheiblehn E	0.4	0.33	0.29	0.13	-17	-11.4	-60.5	-55.4	-67.2	2
OE	44	Ö. Scheiblehn W	0.32	0.22	0.17		-30.2	-22.6				2
OE	45	W. Scheiblehn	0.42	0.37	0.27		-10.3	-26.7				2
OE	46	Hangender	0.23	0.23	0.17		1.5	-24.9				2

Table B.9: Glacier area of all 117 glaciers for the years 1969, 1985, 1997, 2003 and the changes for the periods 1969 - 1985, 1985 - 1997, 1985 - 2003, 1997 - 2003 and 1969 - 2003.

WGS-Code		Name	Area /km <sup>2</sup>			Change /%					Class	
FL	No		'69	'85	'97	'03	69-85	85-97	85-03	97-03		69-03
OE	47	Kitzkamp E	0.37	0.37	0.3		2.1	-18.7				2
OE	48	Kitzkamp W	0.27	0.29	0.17	0.06	8.9	-39.7	-80.7	-67.9	-78.9	2
OE	49	Schrakar	0.23	0.23	0.04		0.4	-80.7				2
OE	50	Haglkar	0.11	0.11	0.06	0.02	5.77	-49.7	-84.1	-68.3	-83.2	2
OE	51	Rötenkar	0.16	0.16	0.08		1.15	-51.4				2
SI	10	NN	0.12	0.05	0.07		-57.4	42.5				2
SI	11	Padreil	0.14	0.12	0.11		-15.8	-9.2				2
SI	12	Simming E	0.21	0.12	0.14		-41.5	13.2				2
SI	13	Simming M	0.69	0.58	0.48		-15.6	-17.9				3
SI	14	Simming W	0.92	0.89	0.68		-2.8	-24.2				3
SI	15	Aperer Feuerstein E1	0.06	0.06	0.04		1.3	-32.4				1
SI	16	Glätte	0.14	0.12	0.12		7-.9	-2.3				2
SI	17	Habicht	0.06	0.06	0.06		3.8	-3.3				1
SI	18	Pinnis	0.06	0.05	0.06		-14.9	5.2				1
SI	19	Äusserer Mischbach	0.26	0.23	0.2		-11.5	-11.3				2
SI	20	Aperer Feuerstein E2	0.21	0.19	0.15		-9.3	-21				2
SI	21	Aperer Feuerstein W	0.14	0.10	0.06		-27.2	-41.3				2
SI	22	NN	0.1	0.1	0.08		1.3	-18.4				2
SI	23	Ö. Grübl	1.15	0.96	0.9		-16.3	-6.8				4
SI	24	Ö. Grübl ob.	0.15	0.14	0.12		-11.5	-8.9				2
SI	25	W. Grübl E	0.4	0.38	0.18		-4.4	-51.1				2

Table B.10: Glacier area of all 117 glaciers for the years 1969, 1985, 1997, 2003 and the changes for the periods 1969 - 1985, 1985 - 1997, 1985 - 2003, 1997 - 2003 and 1969 - 2003.

WGS-Code		Name	Area/km <sup>2</sup>			Change/%				Class		
FL	No		'69	'85	'97	'03	69-85	85-97	85-03		97-03	69-03
SI	26	W. Grübl M	0.23	0.18	0.14		-22.9	-24.2				2
SI	27	W. Grübl W	0.64	0.74	0.6	0.45	15.4	-18.8	-38.9	-24.8	-29.5	3
SI	28	NN	0.07	0.08	0.06	0.02	15.4	-25.5	-70.8	-60.8	-66.3	1
SI	29	Kleiner Grünau	0.15	0.12	0.1		-24.8	-15.5				2
SI	30	Grünau	1.83	1.84	1.7	1.44	0.83	-7.5	-22.1	-15.8	-21.5	4
SI	31	Aperer Freiger	0.38	0.37	0.24	0.09	-2.3	-34.7	-76.2	-63.6	-76.8	2
SI	32	Sulzenau	4.76	4.87	4.56	4.09	2.5	-6.5	-16.2	-10.4	-14.1	4
SI	33	NN	0.14	0.12	0.07	0.05	-12.9	-42.9	-62.1	-33.6	-67	2
SI	34	Fernau	1.94	1.99	1.69	1.43	2.66	-15.2	-28.5	-15.7	-26.6	4
SI	35	Schaufel	1.72	1.69	1.42	1.15	-1.6	15.9	-31.7	-18.8	-32.8	4
SI	36	Daunkogel	1.47	1.59	1.38	1.19	8.1	-13.4	-24.9	-13.3	-18.8	4
SI	37	Daunkopf	0.59	0.54	0.41	0.18	-7.8	-24	-67.5	-57.2	-69.9	3
SI	38	Grosser See	0.17	0.19	0.17	0.06	12.8	-11.7	-69.6	-65.6	-65.7	2
SI	39	Hölltal	0.34	0.24	0.22	0.12	-30.3	-6.1	-51.3	-48.2	-66.1	2
SI	40	Ruderhof u.	0.15	0.15	0.16		1.5	9.7				2
SI	41	Ruderhof o.	0.07	0.07	0.07		8.34	-4.6				1
SI	42	Grabawand	0.45	0.40	0.38		-10.2	-3.8				2
SI	43	Hochmoos	1.41	1.29	1.23		-8.6	-4.9				4
SI	44	Falbesoner Kräul	0.27	0.23	0.24	0.14	-13.3	-4.7	-39.5	-42.2	-47.5	2
SI	45	NN	0.08	0.08	0.07	0.05	-7.55	-2.97	-33.4	-32.4	-38.4	1
SI	46	Falbesoner Knoten	0.39	0.42	0.35	0.25	7	-16.3	-41.3	-29.8	-37.2	2

Table B.11: Glacier area of all 117 glaciers for the years 1969, 1985, 1997, 2003 and the changes for the periods 1969 - 1985, 1985 - 1997, 1985 - 2003, 1997 - 2003 and 1969 - 2003.

WGS-Code		Name	Area/km <sup>2</sup>				Change/%				Class	
FL	No		'69	'85	'97	'03	'69-85	85-97	85-03	97-03		69-03
SI	47	Jedlasgrübl	0.07	0.06	0.06		-14.9	-4.5				1
SI	48	Gugeliger	0.16	0.13	0.12		-23.9	-2.9				1
SI	49	Knotenspitz E	0.11	0.12	0.09	0.05	3.13	-19.8	-53.5	-42.1	-52.1	2
SI	50	Knotenspitz M	0.15	0.06	0.09		-60.1	57.64				2
SI	51	Knotenspitz W	0.09	0.03	0.05		-66.6	68.1				1
SI	52	Sommerwand	0.91	0.58	0.77	0.65	-3.4	-12.9	-25.8	-14.7	-28.2	3
SI	53	Alpeiner Kräul	0.51	0.56	0.48	0.36	12.2	-14.9	-36.2	-25	-28.4	3
SI	54	Seespitz	0.3	0.34	0.24	0.13	12	-29.4	-60.4	-43.9	-55.6	2
SI	55	Alpeiner	3.7	3.73	3.39	3.03	0.9	-9.1	-18.7	-10.6	-17.9	4
SI	56	Verborgen Berg	0.87	0.91	0.79	0.63	4.7	-12.9	-30.9	-20.8	-27.8	3
SI	57	Turm	0.23	0.28	0.18	0.17	20.9	-35.5	-40.5	-7.7	-27.9	2
SI	58	Berglas	0.89	0.89	0.85	0.68	0.14	-5.3	-23.8	-19.5	-23.6	3
SI	59	Berglas N	0.11	0.13	0.09	0.01	21.2	-32	-91.2	-87.1	-89.4	2
SI	60	Lisenser Berglas	0.42	0.39	0.39	0.35	-7.4	2	-9.6	-11.4	-16.3	2
<b>Total</b>			<b>63.05</b>	<b>62.3</b>	<b>53.99</b>	<b>36.86</b>	<b>-1.2</b>	<b>-13.3</b>	<b>-17.6</b>	<b>-10.4</b>	<b>-17.2</b>	

Table B.12: Glacier area of all 117 glaciers for the years 1969, 1985, 1997, 2003 and the changes for the periods 1969 - 1985, 1985 - 1997, 1985 - 2003, 1997 - 2003 and 1969 - 2003.





# Appendix C

## EASI scripts

### Landsat 5 TM

#### Ratio and glacier mask

```
!*****  
!*Workflow to obtain image ratio and glacier mask*  
!*****
```

```
EASI>s rtr
```

```
RTR      Real Database Channel Ratioing      V9.0 EASI/PACE  11:52 22Nov2005
```

```
FILE      - Database File Name              = "850930ratio.pix  
CNUM      - Channels for Ratio Numerator     = 4  
WNUM      - Weights for Ratio Numerator     = 1  
NCON      - Constant for Ratio Numerator    = 0  
CDEN      - Channels for Ratio Denominator  = 5  
WDEN      - Weights for Ratio Denominator   = 1  
DCON      - Constant for Ratio Denominator  = 0  
DBOC      - Database Output Channel List    = 8  
SMOD      - Scaling Mode: NONE/AUTO/LOGS    = "NONE  
MASK      - Area Mask (Window or Bitmap)    =  
ZERODIV   - Value for Division by Zero     =
```

```
EASI>r rtr
```

```
EASI>s thr
```

```
THR      Thresholding Image to Bitmap      V9.0 EASI/PACE  12:01 22Nov2005
```

```

FILE      - Database File Name           = "850930ratio.pix
DBIC      - Database Input Channel List  = 8
DBOB      - Database Output Bitmap       = 9
TVAL      - Threshold Value (Min,Max)    = 2
COMP      - Complement: ON/OFF          = "OFF
DBSN      - Database Segment Name        = "mask1
DBSD      - Database Segment Descriptor  = "glacier mask with THR >= 2.0

```

## Debris

```

!*****
!*Workflow to obtain debris cover on glaciers*
!*****

```

```

!*****
!*Using the EASI modelling tool in Imageworks*
!*****

```

```

if ( %9 >= 130 and %9<=191) then    !%9= Hue component of IHS 345
%%1=1                                !generates mask for whole glacier
else
%%1=0
endif

```

```

%%3= %%1 - %%2                        !%%2=Glacier mask of Ratio TM4/TM5
!%%3=Debris mask

```

## ASTER

### Ratio and glacier mask

```
!*****
!*Workflow to obtain image ratio and glacier mask*
!*****
```

```
EASI>s rtr
```

```
RTR      Real Database Channel Ratioing      V9.0 EASI/PACE  11:52 22Nov2005
```

```
FILE      - Database File Name              = "08232003ratio.pix
CNUM      - Channels for Ratio Numerator     = 3
WNUM      - Weights for Ratio Numerator     = 1
NCON      - Constant for Ratio Numerator    = 0
CDEN      - Channels for Ratio Denominator  = 4
WDEN      - Weights for Ratio Denominator   = 1
DCON      - Constant for Ratio Denominator  = 0
DBOC      - Database Output Channel List    = 6
SMOD      - Scaling Mode: NONE/AUTO/LOGS    = "NONE
MASK      - Area Mask (Window or Bitmap)    =
ZERODIV   - Value for Division by Zero     =
```

```
EASI>r rtr
```

```
EASI>s thr
```

```
THR      Thresholding Image to Bitmap      V9.0 EASI/PACE  12:01 22Nov2005
```

```
FILE      - Database File Name              = "08232003ratio.pix
DBIC      - Database Input Channel List     = 6
DBOB      - Database Output Bitmap         = 7
TVAL      - Threshold Value (Min,Max)      = 2
COMP      - Complement: ON/OFF             = "OFF
DBSN      - Database Segment Name          = "mask1
DBSD      - Database Segment Descriptor    = "glacier mask with THR >= 2.0
```

## Debris

```
!*****
!*Workflow to obtain debris cover on glaciers*
!*****

!*****
!*Using the EASI modelling tool in Imageworks*
!*****

if ( %3 >= 26 and %4<=26) then      !%3, % 4= ASTER channel 3 and 4
%%1=1                               !generates mask for whole glacier
else
%%1=0
endif

%%3= %%1 - %%2                      !%%2=Glacier mask of Ratio A3/A4
                                   !%%3=Debris mask
```

# Appendix D

## Example of Transfer Files

### **alpeinerferner\_session.shp and .dbf File**

Regional Center ID: 11  
Regional Center coordinates: 11.4 E, 47.2667 W  
analysis completion: November 2005  
data source: ASTER image of 23 August 2003 and Landsat  
5 TM of 30 September 1985  
description of processing: data processed using **GLIMS Algorithm  
Working Group** (Kääb, 2004) suggestions  
Analysts surname: Schicker  
Analysts given name: Irene

### **alpeinerferner\_glacier.shp**

glacier ID: SI 55  
location of glacier: 11.1283 E, 47.0466 W  
name of glacier: Alpeiner Ferner

### **alpeinerferner\_outlines.shp**

The .dbf file contains the vector points of the shapefile.

The alpeinerferner\_centrelines.shp, alpeinerferner\_snowlines.shp and alpeinerferner\_debrislines.shp are similar to the alpeinerferner\_outlines.shp file.

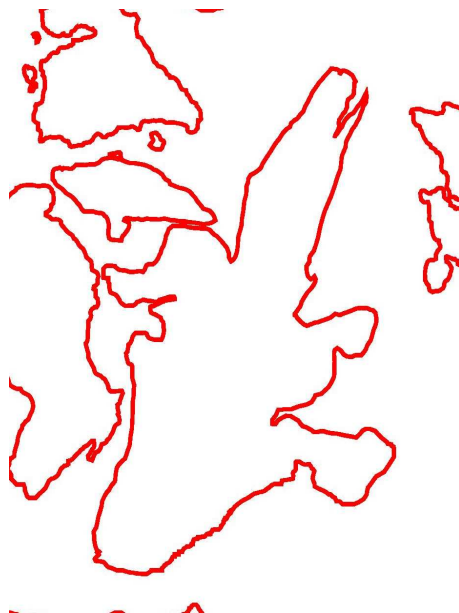


Figure D.1: Alpeiner Ferner glacier boundary in red (alpeinerferner\_outline.shp).

The geoTIFF image screenshot is displayed in figure D.2 .

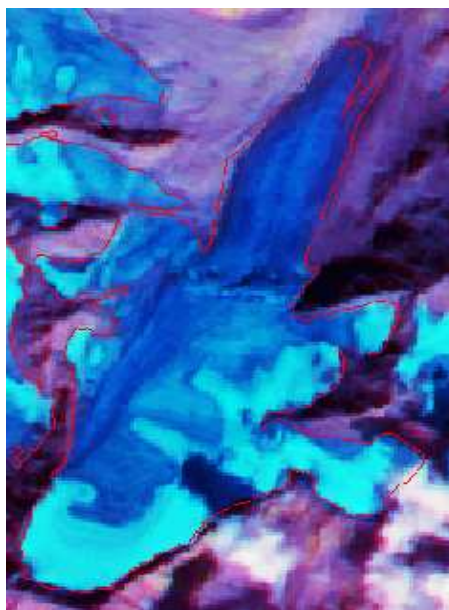


Figure D.2: geoTIFF image of the Alpeiner Ferner with glacier boundaries in red.

# Acknowledgements

At first I have to thank my supervisor Dr. Helmut Rott for giving me the opportunity to gain a new perspective on disappearing glaciers. Special thanks go to Petra, who supported me with geolocation of the satellite data. I have to mention Dana for her support in programming. Furthermore I have to thank Florian for his help with Latex and Claudia for her comments and hints in programming.

Special thanks go to Astrid who helped me with the Austrian Glacier Inventories, ArcGis and helped me getting through many other difficulties.

Thanks go to Gabi, Vevi, Hedwig, Andi, ... for having fun during the last years.

Finally, I am deeply greatfull to my family, who supported me in many ways.